PCCP

Matrix Effect on Hydrogen Bonding and Proton Transfer in Fluoropyridine - HCl Complexes

SCHOLARONE™
Manuscripts

Matrix Effects on Hydrogen Bonding and Proton Transfer in Fluoropyridine - HCl Complexes

Camilla Soares, Anna R. Ley, Brittany C. Zehner, Patrick W. Treacy, and James A. Phillips*

Department of Chemistry and Biochemistry
University of Wisconsin – Eau Claire
Eau Claire, WI 54702

* Author to whom correspondence should be addressed:

email:　　　　phillija@uwec.edu
phone:　　　　715-836-5399
fax:　　　　　715-835-4979

Abstract

We report an extensive computational and spectroscopic study of several fluoropyridine–HCl complexes, and the parent, pyridine-HCl system. Matrix-IR spectra for pentafluoropyridine–HCl, 2,6-difluororpyridine–HCl, and 3,5-difluororpyridine–HCl in solid neon exhibit shifts for the H-Cl stretching band that parallel the effects of fluorination on hydrogen-bond strength. Analogous spectral shifts observed across various host environments (solid neon, argon, and nitrogen) for pentafluoropyridine–HCl and 2,6-difluororpyridine–HCl convey a systematically varying degree of matrix stabilization on the hydrogen bonds in these complexes. An extended quantum-chemical study of pyridine-HCl and eight fluorinated analogs, including 2-, 3-, and 4-fluoropyridine–HCl, 2,6- and 3,5-difluoropyridine–HCl, 2,4,6- and 3,4,5-trifluropyridine–HCl, as well as pentafluoropyridine–HCl, was also performed. Equilibrium structures and binding energies for the gas-phase complexes illustrate two clear trends in how fluorine substitution affects hydrogen bond strength; increasing fluorination weakens these interactions, yet substitution at the 2- and 6-positions has the most pronounced effect. Bonding analyses for a select subset of these systems reveal shifts in electron density that accompany hydrogen bonding, and most notably; the values of the electron density at the N--H bond critical points among the stronger systems in this subset significantly exceed those typical for moderately strong hydrogen-bonds. We also explored the effects of dielectric media on the structural and bonding properties of these systems. For pyridine-HCl, 3-fluoropyridine–HCl, and 3,5-difluororpyridine–HCl, a transition to proton transfer-type structures is observed at ε-values of 1.2, 1.5, and 2.0, respectively. This is signaled by key structural changes, as well as an increase in the negative charge on the chorine, and dramatic shifts in topological properties of the H-Cl and N--H bonds. In the case of pentafluoropyridine–HCl, and 2,6-difluororpyridine–HCl, we do not predict proton transfer in dielectric media up to ε=20.0. However, there are clear indications that the media enhance hydrogen-bond strength, and moreover, these observations are completely consistent with the experimental IR spectra.

Introduction

Because hydrogen bonding is known to play a vital role in a wide range of natural phenomena, studies of its fundamental aspects have been so prevalent that numerous monographs (1-4) and reviews (5-13) have been published, and these span several decades. A key, persistent issue within this broader context regards the transition between hydrogen bonding and proton transfer, and in particular, the conditions by which the former (an *interaction*) becomes the latter (a *reaction*) (13). In a recent review, Grabowski asserts that proton transfer follows from some degree of covalent character in the hydrogen bond, which has been illustrated via topological analyses (8, 11, 14) (which have been questioned (15)), but also in some cases via energy decomposition analyses (14-19). Also in the review, Grabowski (13) presents a series of solid-state structures involving O-H--O interactions that depict a continuous structural transition; these data effectively map out a reaction path for the intermolecular proton-transfer process, as mediated by a hydrogen bonding interaction. However, recent, groundbreaking results counter this notion of a continuous transition between hydrogen bonding and proton transfer (20). In a study of the classic F_2H^- system via ultrafast, time-resolved 2-D IR spectroscopy and high-level theory, the key structural and electronic properties were mapped along a reaction coordinate (F--F) spanning structures across the entire range from hydrogen bonding to covalent bonding – *i.e.*, *within a single system.* Interestingly, they identified a key point on this reaction coordinate that seemed to mark key changes signaling a *distinct* transition between hydrogen bonding and covalent (3-center-4-electron) bonding.

In any event, the notion of a continuous transition between hydrogen bond and proton transfer, at least across a series of analogous systems, has persisted in the literature for decades, and is implicit in one of the earliest classification schemes presented by Ault (21). Within this framework, there are three types of interactions between an H-bond donor (HA) and an H-bond acceptor (B): "Type I" hydrogen bonds (B--H-A) at one extreme, "Type III" proton-transfer complexes (*i.e.*, B-H$^+$…A$^-$) at the other, and intermediate, "Type II" or "proton-shared" cases (B--H--A) that lie within these limits. The amine-

hydrogen halide complexes (*e.g.*, H$_3$N–HCl, (CH$_3$)$_3$N–HBr, etc.) (22-24), provide illustrative examples of these cases, and are closely related to the present work. At the Type I extreme lies H$_3$N–HF, a strong, hydrogen-bonded complex. By contrast, (CH$_3$)$_3$CN–HBr is a Type-III complex in which there is nearly complete transfer of a proton (*i.e.*, (CH$_3$)$_3$CNH$^+$ Br$^-$). Other systems in this series exhibit intermediate degrees of proton transfer, which increases with the size of halogen (Br > Cl > F), and the extent of methylation in the amine ((CH$_3$)$_3$N > H$_3$N) (22).

Among these complexes, H$_3$N–HCl is arguably the most extensively studied (25-31), and matrix-IR results for this system demonstrate that hydrogen bond strength, and the extent of proton transfer, can also be facilitated by interactions with the surrounding chemical environment. Early studies on H$_3$N–HCl in argon and nitrogen matrices (32, 33), found the HCl band was substantially red-shifted, and split into two components, consistent with a Type II, proton-shared interaction. However, when the IR spectrum of H$_3$N–HCl was revisited years later in solid neon (29, 30), a distinct ν_{HCl} band was observed, still significantly red-shifted from the free HCl band, but much less so than in the argon-matrix spectrum. The upshot was that the extent of proton transfer was very much dependent on matrix host; a slight shift in "solvent stabilization" from solid neon, to argon, to nitrogen manifested a major change in structure, characterized by a transition from hydrogen bonding to proton transfer.

Theoretical studies provided further support for the occurrence of matrix-facilitated proton transfer. In an MP2 study of the 2-D (E vs N--H and H-X) potential surface for H$_3$N–HCl (34), the gas-phase minimum was consistent with a Type I, hydrogen-bonded structure. However, when matrix effects were simulated via an applied electric field, the minimum shifted sequentially toward the Type II portion of the curve with increasing field strength (34). In turn, analysis of vibrational motion along the proton-stretching coordinate along this yielded good agreement with experimental matrix spectra (25, 26). More recently, our group (31) was able to illustrate the transition between H-bonding and proton transfer for H$_3$N–HCl in low-dielectric media using a more simplistic 1-D potential curve (E vs. N--Cl

4

distance). Also in that study, we documented experimental shifts in the ν_{HCl} band for CH$_3$CN–HCl, and

through an analogous modeling approach were able to illustrate that these spectral shifts were

consistent with a medium-induced strengthening of the hydrogen bond, rather than the onset of proton

transfer to any significant degree (31). Nonetheless, analogous effects have been shown to be

significant for interactions between DNA base pairs (18, 35).

Analogous studies of pyridine-HCl (16, 32, 33, 36-38) and its analogs (37, 39-42) have been

somewhat less definitive, and moreover, the interpretation of the experimental matrix-IR results has

been complicated because the host environments tend to enhance the extent of proton transfer and

induce mode coupling that impedes direct comparisons with standard quantum-chemical frequency

predictions. The pyridine-HCl complex has been studied by rotational spectroscopy (36), and these

results convey a strongly hydrogen-bonded complex, with a fairly short N-H distance, and at most only

a slight degree of proton transfer. In a somewhat recent MP2 study (16), electrostatic forces were found

to make the most significant contribution to the binding energy, though the agreement with the

experimental structure (36) was marginal. By contrast, prior observations of pyridine-HCl in argon

matrices (32) noted two groups of strong bands attributed to the "proton stretching" motion, lying below

1000 cm^{-1} and thus extensively shifted from the parent HCl stretch at about 2900 cm^{-1}. The

interpretation was that this system had a "proton shared" (Type II) hydrogen bond, but the difficulty of

inferring the position of the H-atom from the spectra was also noted (32).

Subsequent efforts by Del Bene and co-workers confirmed and expanded upon these early

observations for pyridine-HCl (37-40), and in addition, these provided evidence for matrix-induced

proton transfer in a set of 4-substitued analogs (*i.e.*, 4-X-pyridine–HCl) (37, 39, 40). Specifically, the

X=CN, Cl, H, and CH$_3$ complexes were predicted to be Type I complexes in the gas phase, but

experimental spectra in argon and nitrogen matrices (32, 37) exhibited dramatic differences from the

computed (harmonic) vibrational spectra (37). Ultimately, anharmonic spectral simulations confirmed

5

early assessments that pyridine-HCl was a proton-shared system in these matrix environments, in which the proton-stretching potential slightly favored a Cl-H--N arrangement for the complex in argon, and a Cl--N-H arrangement in nitrogen, but would also be subject to large amplitude vibrational motion that blurs these distinctions (37). This assessment was subsequently reaffirmed by a thorough ab initio (MP2/aug-cc-pVTZ) mapping of the 2-D potential for the proton stretching coordinate (*i.e.*, E vs. Cl-H and N-H) for pyridine-HCl, in which the matrix effects were represented by an applied electric field (38).

In this manuscript, we present a series of matrix-IR and quantum chemical investigations of pyridine-HCl and several of its fluoropyridine analogs. Previous computational studies (MP2) on fluoropyridine-HCl complexes (41, 42) have shown that fluorination acts to weaken the hydrogen bonds, and substitution adjacent to the nitrogen has a more preround effect. This effect has also been shown to impact interactions in non-native DNA base pairs (18). Here, we not only revisit how fluorine substitution affects strength and structure, we also explore how it manifests trends in the electron distribution through the hydrogen-bond linkages (N--H-Cl) in these systems, as well as their response to condensed-phase media. In the experimental phase of this work, we conducted a series of matrix-IR experiments, which were focused on the weaker systems as to avert the spectral complications arising from the onset of proton transfer noted above. In these, we observed shifts in the ν_{HCl} bands of 2,6-dilfuroropyridine-HCl, 3,2-dilfuroropyridine-HCl, and pentafluoropyridine-HCl across various matrix hosts, including solid neon, argon, and nitrogen. For the quantum-chemical portion of this study, we explored a much larger set of complexes, including pyridine-HCl and eight fluorinated analogs, which span the range of interaction strengths that extends beyond those discussed above (37, 39-42). For these, we obtained structures, binding energies, and frequencies for the gas-phase systems. We also conducted bonding analyses, and assessed the effects of bulk, dielectric media via continuum solvation modeling. Most notably, we predict that the stronger complexes transition to proton-transfer structures in low-dielectric media, and moreover, bonding analyses seem to indicate some key distinctions between these and the systems that do not make this transition.

Methods

Materials

Liquid pentafluoropyridine (>99%), 2,6-difluoropyridine (99%), and 3,5-difluorpyridine (97%) were obtained from Sigma-Aldrich, and gas mixtures for matrix isolation experiments were made by drawing the ambient vapor of each compound. To accomplish this, each sample was transferred to a 25 mL sample tube (Chemglass AF-0092), connected to a preparatory gas manifold (Chemglass AF-0300-03), and then purified via several freeze-pump-thaw cycles immediately prior to mixture preparation. HCl gas (Matheson), DCl (Matheson), as well as neon (Praxair, >99.999%), argon (Praxair, 99.9999%) and nitrogen (Praxair, 99.9999%) were used without any further purification. Gas mixtures were prepared in 2-L glass bulbs (Chemglass, AF-0093), with guest-host ratios ranging from 1/400 to 1/1600, using a preparatory manifold that maintained at or below a pressure of 2×10^{-4} torr using a glass diffusion pump (Chemglass AF-0300-03). For DCl experiments, the inner surface of a 2-L glass bulb was rinsed with ~3 mL of liquid D_2O (Acros, 99.8%) then attached to the preparatory manifold, and heated for 24 hours to facilitate H/D exchange on the inner surfaces. In spite of the this, the DCl-seeded matrix samples most often contained a significant fraction of HCl, which varied, and tended to increase as the mixture was used over 2 to 3 days. In the end, this turned out to be advantageous in one respect, as it enabled us to display both H- and DCl spectra in a single trace (and the H/D isotopes shifts are substantial, such that overlapping H-D bands was not an issue).

Low – temperature infrared spectra

Matrix isolation-IR experiments were performed on an apparatus described previously (43). Matrix samples were prepared by flowing H/DCl and fluoropyridine mixtures through separate Teflon lines connected with stainless steel compression fittings. The plumbing configuration keeps the acid and base these lines separated (as to prevent the formation of bulk fluoropyridinium chlorides in the deposition lines), until they merge as they enter the cryostat vacuum chamber, immediately prior to deposition onto a gold-plated mirror. Neon matrices were deposited at 6K, in several 30 to 60-minute

intervals, with flow rates ranging from 3 to 12 mmol/hr. Most were subsequently annealed at 8 to 9K for

several 30-minute intervals. Argon and nitrogen matrices were deposited at temperatures between 14

and 20K, and annealed at 27 to 32 K. Flow rates were controlled using Granville-Phillips #203 leak

valves, and temperatures were controlled using a Lakeshore 331 temperature controller with two silicon

diodes, one at the end of the cold head, one immediately behind the sample on the back side of the

mirror). Spectra were recorded after each deposition or anneal interval using a Thermo Nicolet Nexus

670 FTIR, at 2 cm^{-1} resolution, and 400 scans were averaged for each spectrum.

Computations

Computations were performed using Gaussian 09, version B.01(44). Equilibrium structures were

obtained via M06 (45), ωB97X-D (46), and MP2 (47), with the aug-cc-PVTZ basis set (47), with

convergence criteria set using "opt=verytight" option and an "ultrafine" integration grid. The rationale for

the stringent geometric convergence criteria stems from an apparently flat intermolecular potential with

respect to the angular orientation of the HCl subunit in these systems. This will be discussed further

below. We conducted our initial geometry searches using M06, as it had been the method of choice in

our recent work on CH_3CN–HCl and H_3N–HCl (31). MP2 was included as to provide a set of post-HF

results for the sake of comparison, and we chose ωB97X-D as it had been effective in several of our

recent studies on Lewis acid-base systems (48, 49). As a whole, the structural results among these

various methods were reasonably consistent, but we ultimately found that ωB97X-D best reproduced

the measured N--Cl distance (36) and CCSD/aug-cc-pVTZ binding energy for C_5H_5N–HCl. As such, we

report the ωB97X-D structures in the figures below, and utilize ωB97X-D on the subsequent bonding

analyses. However, N--H distances and complex binding energies are reported below for all three

methods, as to facilitate a comparison of methods. Atomic charges were obtained via Natural

Population Analyses (NPA) (50), and for a select sub-set of these complexes we conducted Atoms in

Molecules (AIM) analyses (51). Both of these bonding analyses were executed directly in Gaussian.

Also, for a select subset of complexes, the effects of dielectric media on the ωB97X-D/aug-cc-pVTZ

were explored using the Polarized Continuum Model (PCM) (52), with a range of dielectric constants (1.2, 1.5, 2.0, 3.0, 5.0, 10.0, and 20.0). The other solvent parameters were left at their default values (*i.e.*, for water). For these optimizations, convergence criteria were relaxed to the "opt=tight" setting, and bonding analyses were also conducted at each ε value.

Results and Discussion

Matrix-IR Spectra

Overall, we collected infrared spectra of matrices containing HCl/DCl, and/or pentafluoropyridine (PFP), 2,6-difluoropyridine (2,6-DFP), or 3,5-difluorpyridine (3,5-DFP) in solid neon, argon, and/or nitrogen. In the analysis and interpretation of these spectra, we focused almost exclusively on the H-Cl (and D-Cl) stretching bands (ν_{HCl}) because they offer the most insight into the strengths of the interactions in the complexes. These bands were readily identified by as a strong, and sometimes rather broad features, red-shifted from the corresponding bands of free (matrix-isolated) HCl and $(HCl)_n$ (53). The overall rationale for the assignment of these peaks to the corresponding 1:1 complexes, stated here in general terms, includes: i) They were, by far, the most prominent product peaks in the spectrum (as is the case with related systems, *e.g.*, $CH_3CN–HCl$ (31), 4-XPYR–HCl (37), and $H_3N–HCl$ (30)), ii) These peaks consistently grew upon annealing; iii) They persist at fairly low concentrations (1/3200 for each guest); iv) There are no additional product bands in the region with comparable intensity. In addition, we also performed isotopic substitution experiments, which confirm the peaks arise from an HCl-containing carrier with predictions based on the reduced mass of HCl (*i.e.*, $\nu_{HCl}/\nu_{DCl} \sim$ 1.4). We also note that the peaks assigned to ν_{HCl} in solid nitrogen were fully discerned only after annealing, which suggests that overall, clustering is not prevalent in this host, and in turn, extensive formation of larger clusters in other hosts at comparable conditions seems unlikely. Furthermore, the experimental shifts ($\nu_{complex}$ - ν_{HCl}) in neon matrices agree reasonably well with (gas-phase) predictions, and the measured frequencies for PFP–HCl and 3,5-DFP–HCl align well with previously assigned bands for $CH_3CN–HCl$ (31). In most cases, additional product bands were observed, which were

9

relatively weak, and shifted only slightly from the signals due to the un-complexed fluoropyridine compound, and were not interpreted further. A few of these have been attributed to larger clusters. Also, there are many, narrows peaks present in a typically sparse region of the spectrum (roughly 2000-2500 cm^{-1}), which are clearly present in the various fluoropyridine control spectra, and we presume that these arise from overtone and combination bands involving the intense C-F stretching modes; though we conducted no analysis to confirm this. There are also impurity CO_2 absorptions in this region (near 2350 cm^{-1}).

Infrared spectra of matrices containing PFP and/or HCl in solid neon are displayed in Figure 1 (left), and in these we observed product bands (those requiring both HCl and the corresponding pyridine compound) at: 2838, 2783, 2747, 2670/2655, 1565, 1461, and 984 cm^{-1}. With mixture of HCl and DCl in the sample, we observe additional peaks at 1991, 1937, 1677, 1304, and 1085 cm^{-1}. By far, the bands at 2747 and 1991 cm^{-1}, are the most prominent features in the spectra, and they are marginally red-shifted from the H/DCl (free, and self-clustering) peaks in the reference spectrum, as would be expected given the relative strengths of the H--Cl and H--N interactions. In addition, the frequencies are also consistent with and H/D isotopic pair for the $\nu_{H/DCl}$ bands. Thus, we assign the bands at 2747 and 1991 cm^{-1}, respectively, to the ν_{HCl} and ν_{DCl} bands of the 1:1 PFP–H(D)Cl complex. Regarding the peaks at 2838 and 2783 cm^{-1}, which were observed only intermittently. These bands essentially coincide with HCl-self clustering peaks, though the relative intensities differed from the self-clustering pattern in the reference, suggesting underlying peaks. In addition, the bands at 2670/2655 (HCl) and 1911 cm^{-1} (DCl) are only observed at higher concentrations, and being further red-shifted from the most prominent bands, are likely due to larger PFP/HCl clusters.

Figure 1. IR spectra of neon matrices containing pentafluoropyridine (PFP) and/or H(D)Cl. Left: HCl/PFP/Ne at guest-host ratios of 1/1/1600; controls at 1/800. Right: H(D)Cl/PFP/Ne at guest host ratios of 2*/1/1600 (*with an approximate 1/1 relative concentration D/H); controls at 1/800 (PFP) and 1/400 H(D)Cl.
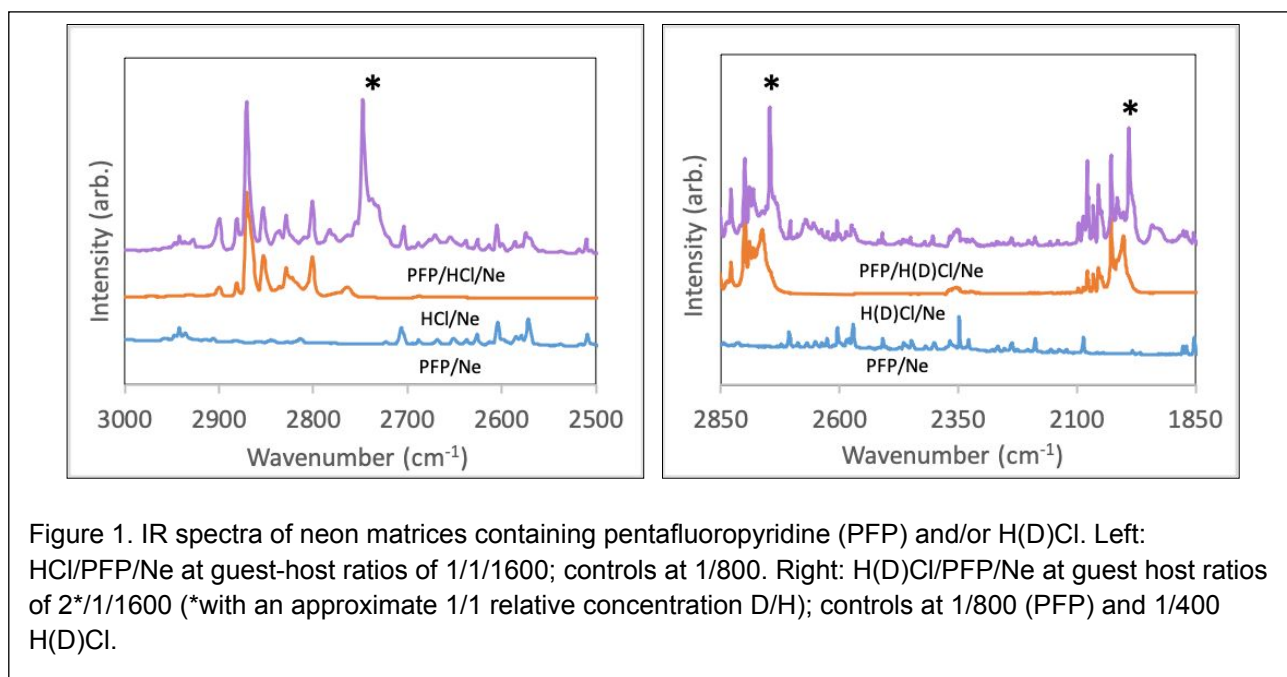
Analogous HCl/PFP spectra in solid argon and nitrogen are displayed in Figure 2. In the argon experiments (*left*), we observed product bands at: 2690, 1498, 1361, and 1084 cm^{-1}. The most intense of these (2690 cm^{-1}) is located in the HCl region, marginally red-shifted from the HCl peaks in the reference trace, and also just to the red of the analogous neon-matrix peak. The band also grows upon annealing. Therefore, we assign it to the ν_{HCl} band for PFP-HCl. In the corresponding nitrogen-matrix spectra (*right*), we observed product bands at 2631, 1567, 1500, 1462, 1435, 1084, 983 cm^{-1}. The most intense product band is 2631 cm^{-1}; which lies in the expected region for the HCl stretch (somewhat more red-shifted than its argon counterpart), and once again grows upon annealing (as shown in Figure 2; it was somewhat obscured after deposition alone). Nonetheless, based on these characteristics, we assign the peak at 2631 cm^{-1} to the ν_{HCl} band of PFP-HCl in solid nitrogen.

1

Figure 2: IR spectra of argon and matrices containing pentafluoropyridine (PFP) and HCl. Left: HCl/PFP/Ar at guest-host ratios of 1/1/1600; controls at 1/800. Right: HCl/PFP/N$_2$ at guest host ratios of 1/800 for the control spectra, and 3/4/5600 for the sample with both HCl and PFP. Dashed line is annealed sample (30 min at 28 K).
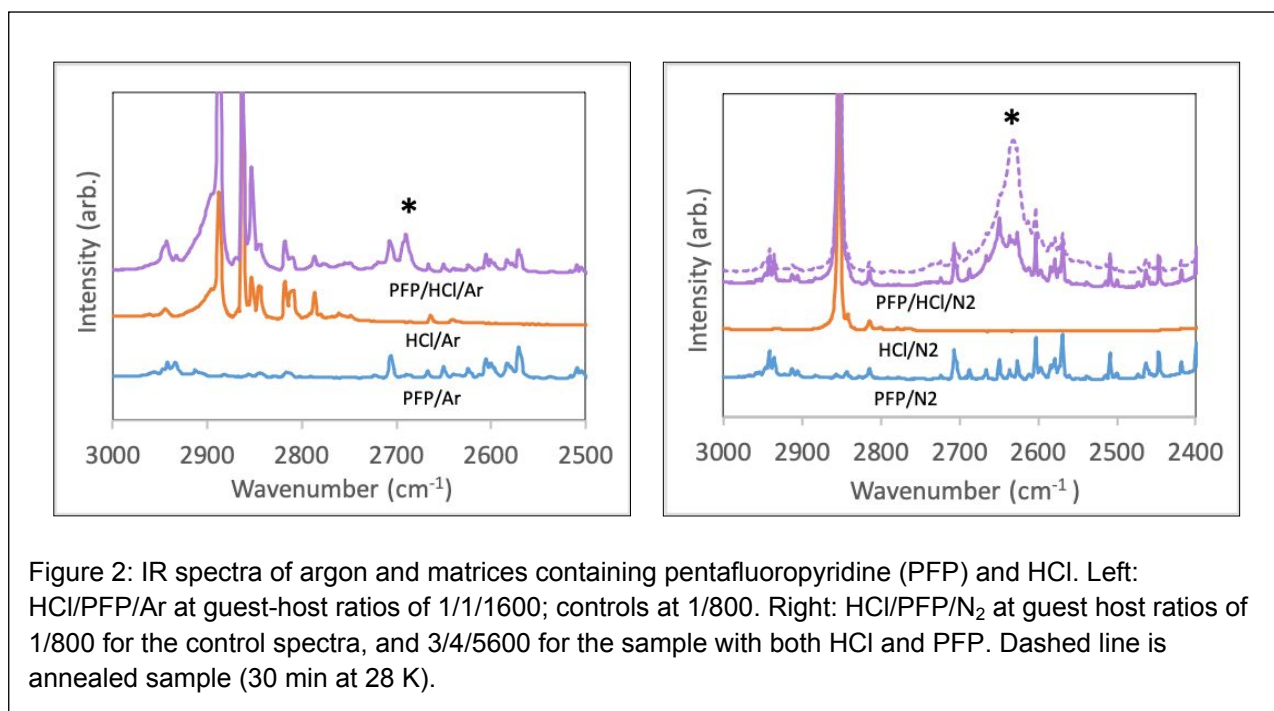
Figure 3 displays the infrared spectra of matrices containing 2,6-DFP and/or H/DCl in solid neon. In the HCl experiments, we observed product bands at: 2627, 1325, 1294, 1248, and 1005 cm^{-1}. Upon deuterating the sample, additional peaks are observed at observed at: 1911, 1810, 1622, 1311, 1232, and 995 cm^{-1}. The most prominent features occur at 2627 and 1911, cm^{-1}; they grow upon annealing, are red-shifted from the H/DCl peaks in the reference, and ratio of these observed frequencies is consistent with an H/D isotopic pair. Thus, we assign the bands at 2627 and 1911 cm^{-1} to the ν_{HCl} and ν_{DCl} bands of 2,6-DF–H(D)Cl, respectively. The 1810 cm^{-1} band (in the DCl/2,6-DFP spectra) is only observed at higher concentrations (and has inconsistent relative intensities with the 1911 cm^{-1} band), suggestive of a larger DCl/2,6-DFP cluster (though we see no analog in the HCl region).

1

Figure 3. IR spectra of neon matrices containing 2,6-difluoropyridine (2,6-DFP) and/or H(D)Cl. Left: HCl/2,6-DFP/Ne at guest-host ratios of 1/1/1600; controls at 1/800. Right: H(D)Cl/2,6-DFP/Ne at guest host ratios 3*/2/4000 for the sample with both HCl and PFP; 2*/800 and 1/800 for the controls, respectively (*with an approximate 1/1 relative concentration D/H).
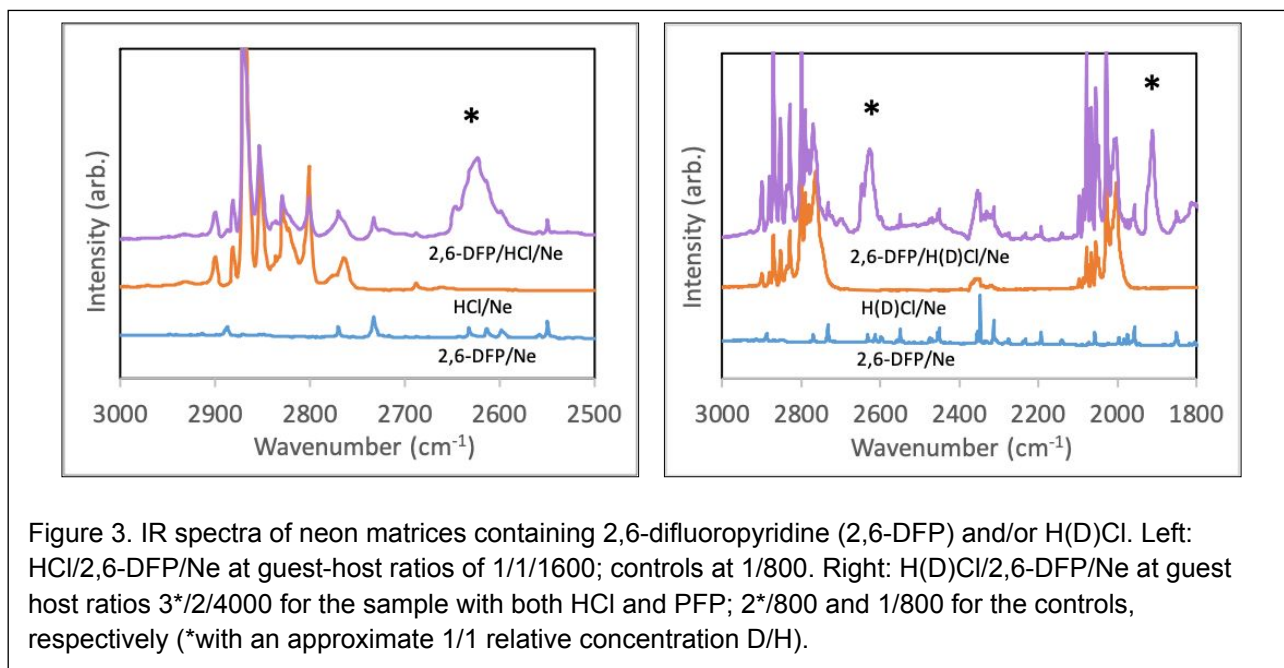
Infrared spectra of argon and nitrogen matrices containing 2,6-DFP and HCl are displayed in Figure 4. In the argon-matrix experiments (*left*), we observed product bands at 2677, 2577, 1321, and 1003 cm^{-1}. The strongest peak (2577 cm^{-1}) lies in the expected H-Cl stretching region, in is red-shifted from absorptions in the HCl reference trace, as well as the ν_{HCl} band in solid neon. Thus, we assign it to the ν_{HCl} band of 2,6-DFP–HCl. In the corresponding nitrogen-matrix experiments (*right*), product bands were observed at 2494, 2390, 1322, 1247, and 1002 cm^{-1}. The 2494 cm^{-1} peak is a broad, high-intensity band, which grows upon annealing and lies somewhat to the red of the peaks in argon and neon. Thus, we assign the 2494 cm^{-1} peak to the ν_{HCl} band of 2,6-DFP–HCl in solid nitrogen. We do not know the origin of the other, fairly intense band that grows in the annelid spectrum, but it seems to be present in the 2,6-DFP/Ne control, at least in part.

Figure 4: IR spectra of argon and matrices containing 2,6-difluoropyridine (2,6-DFP) and HCl. Left: HCl/2,6-DFP/Ar at guest-host ratios of 1/1/1600; controls at 1/800. Right: HCl/PFP/N_2 at guest host ratios of 1/800 for the control spectra, and 2/3/4000 for the sample with both HCl and 2,6-DFP. Dashed line is annealed sample (30 min at 28 K).
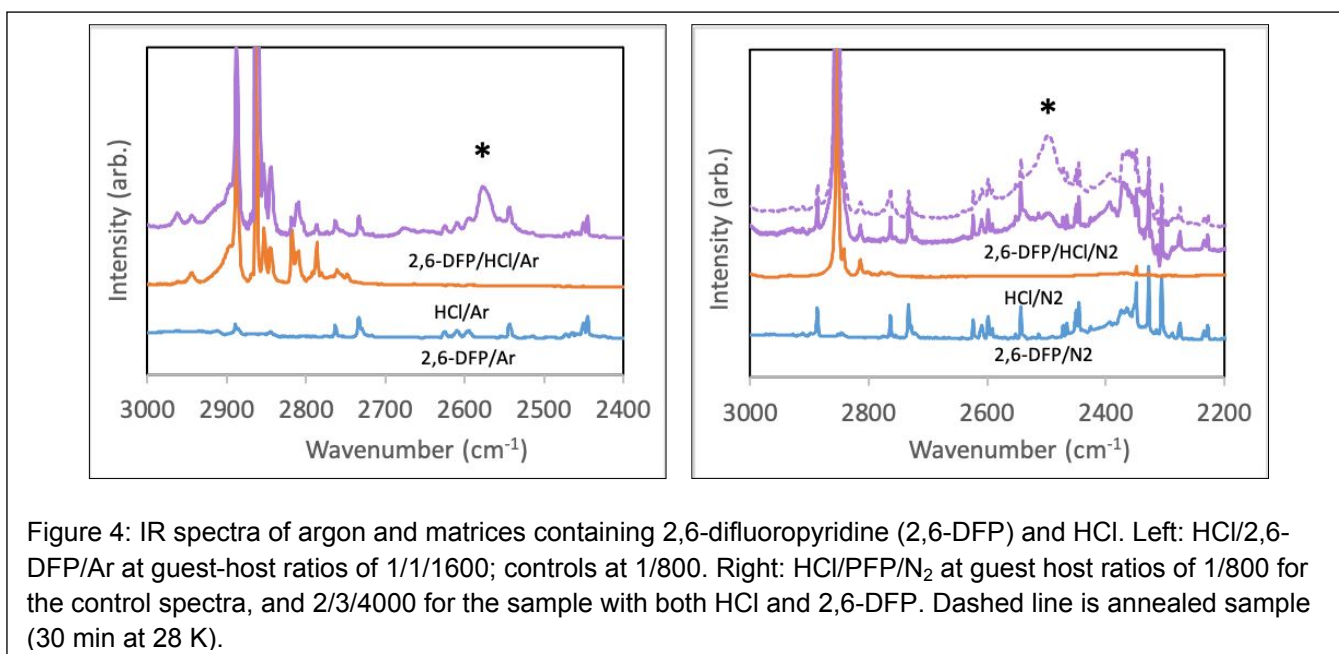
Infrared spectra of matrices containing 3,5-DFP and/or HCl in solid neon are displayed in Figure 5. These spectra are dominated by intense, broad absorption features. In the HCl spectra (*left*), this ranges from 2497-1864 cm^{-1}, well red-shifted from the peaks in the HCl reference spectrum, with two maxima at 2241 and 2021 cm^{-1}. Analogous features were noted in the DCl experiments (*right*), in the low-frequency portion of the DCl stretching region, with two maxima at 1735 cm^{-1} and 1607 cm^{-1}. These frequencies are largely consistent with the expected H-D isotopic shift for the ν_{HCl} band, which seems to indicate that these broad features correspond to the ν_{HCl} and band of 3,5-DFP–HCl. However, it is not immediately clear as to why these absorption bands are so broad, or why they exhibit two absorption maxima. As such, a definitive assignment is difficult. One might expect the feature to broaden with the onset of proton transfer, and in the work on analogous systems (37, 39, 40), mode coupling led to additional bands corresponding to the proton stretching motion, but in these instances the peaks were much further shifted to the red. We had also considered that these my arise from bulk 3,5-diflouropyridinium chloride, but the broad, strong N-H stretching peak for sold pyridinium chloride is centered just below 3000 cm^{-1} (54). In the absence of any definitive explanation of these observations,

1

we offer only a tentative assignment, and further, we did not pursue argon and nitrogen spectra for the 3,5-DFP–HCl studies.

Figure 5. IR spectra of neon matrices containing 3,5-difluoropyridine (3,5-DFP) and/or H(D)Cl. Left: HCl/3,5-DFP/Ne at guest-host ratios of 1/1/1600; controls at 1/800. Right: H(D)Cl/2,6-DFP/Ne at guest host ratios of 1/800 and 2*/800 for the control spectra of 3,5-DFP and H(D)Cl, respectively, and 2*/1/2400 for the sample with both H(D)Cl and 3,5-DFP (*with an approximate 1/1 relative concentration D/H).
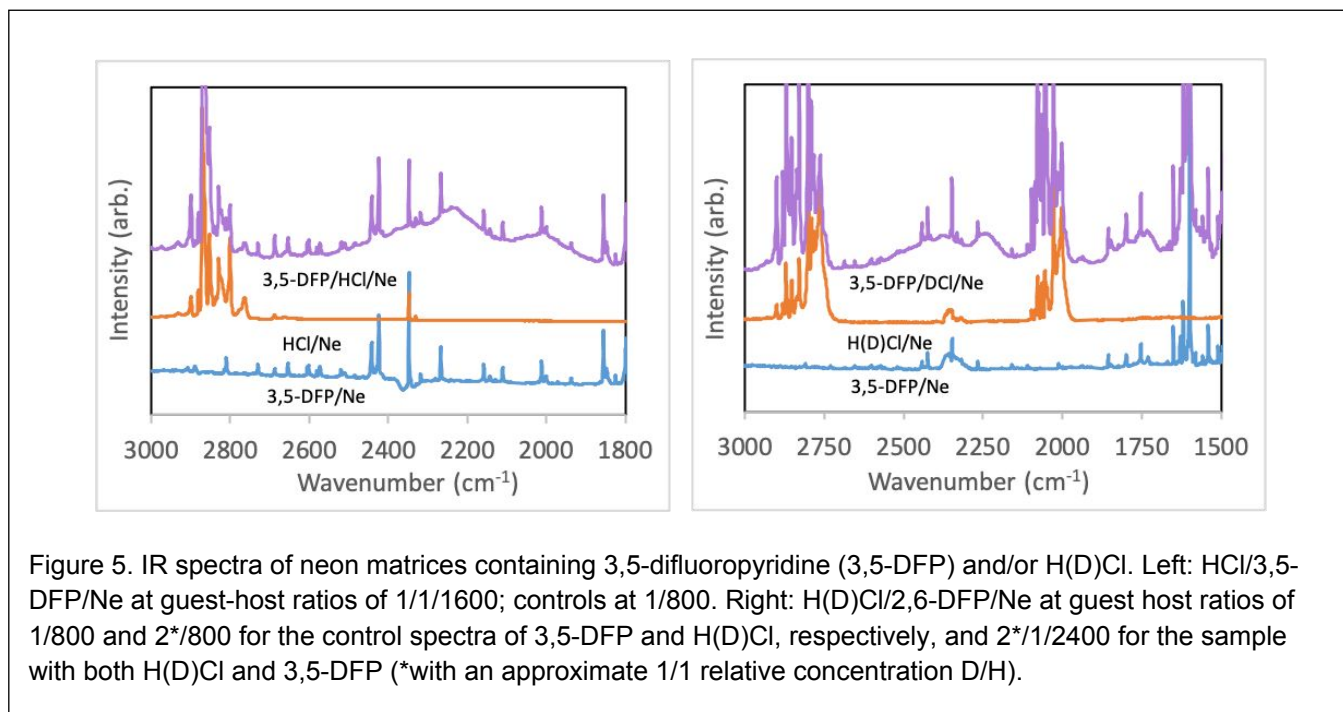
Frequency shifts

The overall shifts of the ν_{HCl} band across three different fluoropyridine complexes (PFP, 2,6-DFP, 3,5-DFP and HCl) in solid neon are shown schematically in Figure 6 (a). The ν_{HCl} bands appear at 2747, 2627 and ~2241 cm^{-1} for the HCl containing matrices of PFP, 2,6-DFP and 3,5-DFP respectively. We observe the frequency corresponding to the weakest base, PFP, laying at the left-most side of the spectrum, and the frequencies for 2,6-DFP-HCl and 3,5-DFP–HCl are red-shifted by about 120 and ~500 cm^{-1}, respectively. These shifts are consistent with the increasing strength of hydrogen bonds in these complexes (PFP < 2,6-DFP < 3,5-DFP), and we note that the neon-matrix frequency for CH$_3$CN–HCl (intermediate in binding energy between PFP–HCl and 2,6-DFP–HCl – *see below*) occurs at 2677 cm^{-1}; as would be expected on the basis of strength. Matrix-induced shifts for PFP–HCl are depicted in Figure 6 (b). The ν_{HCl} band for this complex is observed at 2690 cm^{-1} in argon, and 2631 cm^{-1} in nitrogen, which are red-shifted by -59 and -116 cm^{-1}, respectively, relative the neon-matrix value (2747

cm^{-1}). The frequencies for 2,6-DFP–HCl span a slightly larger range, and are illustrated in Figure 6 (c). In this case, the ν_{HCl} bands are observed at 2627, 2577, and 2497 cm^{-1} in solid neon, argon, and nitrogen, respectively. Here, the argon- and nitrogen-matrix values are red-shifted by -50 and -130 cm^{-1}, respectively, in comparison to the neon-matrix frequency. The observed trends in these matrix-induced shifts (Ne < Ar < N$_2$), indicates that the medium causes a systematic strengthening of the hydrogen bonds and, moreover, that the subtle differences in solvent stabilization offered by these inert media manifest significant differences in the extent to which they enhance the hydrogen-bonding interactions. In addition, the stronger complex (2,6-DFP–HCl) appears to be slightly more sensitive to these subtle differences in "solvent" stabilization. Again, the data for CH$_3$CN–HCl are intermediate between the PFP–HCl and 2,6-DFP–HCl frequencies in both argon and nitrogen (31, 55), which is also consistent with the apparent trend between strength and medium sensitivity.

1

Physical Chemistry Chemical Physics

a)

b)

c)

Figure 6: Frequency shift schematics: a) Neon-matrix frequencies of the ν_{HCl} bands for PFP–HCl, 2,6-DFP–HCl, and 2,3-DFP–HCl; b) Frequencies of the ν_{HCl} band of PFP–HCl in solid neon, argon, and nitrogen; c) Frequencies of the ν_{HCl} band of 2,6-DFP–HCl in solid neon, argon, and nitrogen.

1
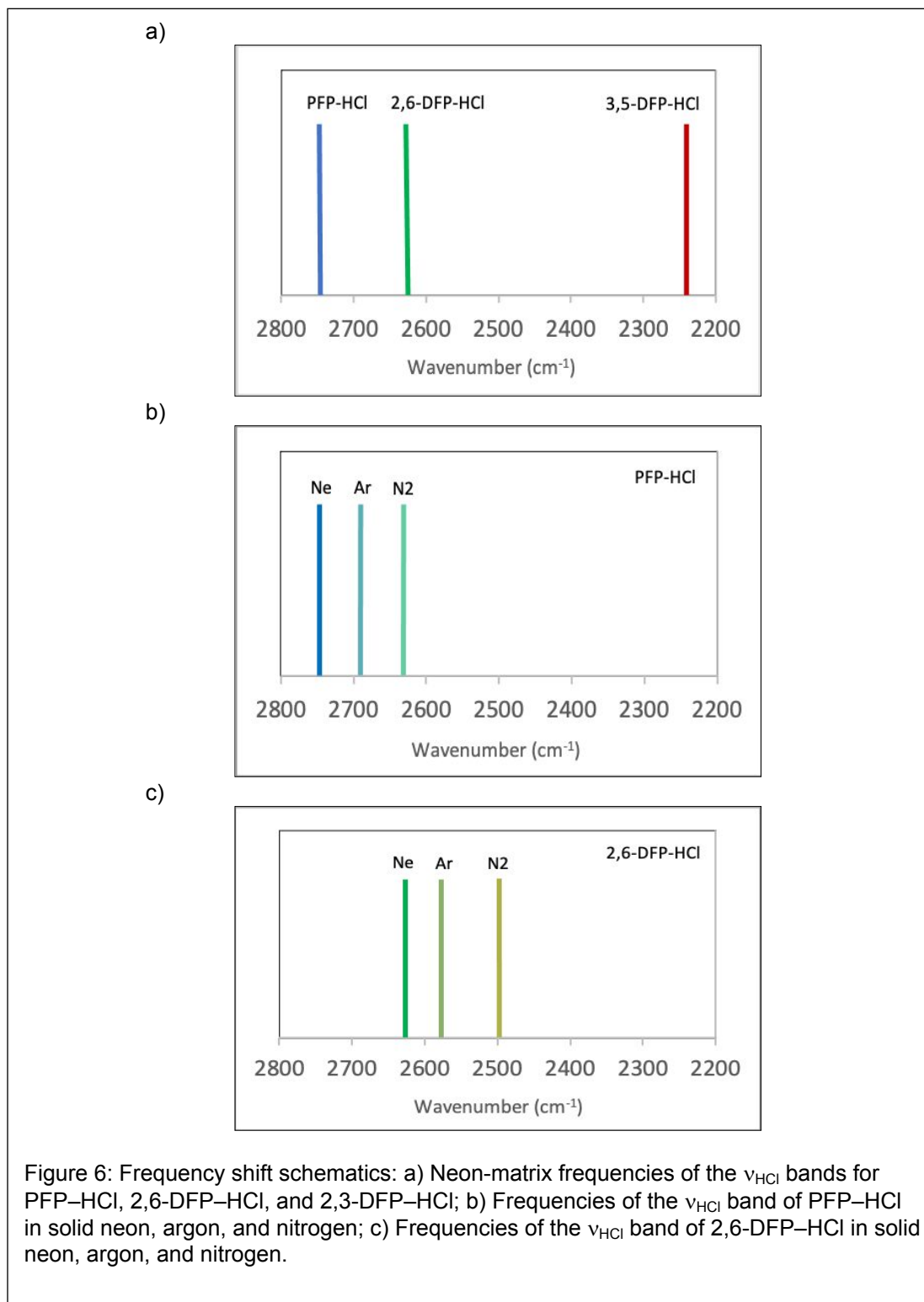
Computations: Structures and Binding Energies

To obtain a broader understanding of the changes in structure and bonding that manifest these differences in measured vibrational frequencies, we undertook an extended quantum-chemical study, which included pyridine-HCl and a set of eight fluorinated analogs. The first step in this analysis was obtaining equilibrium structures and binding energies for the HCl complexes of: pyridine (PYR), 2-fluoropyridine (2FP), 3-fluoropyridine (3FP), 4-fluoropyridine (4FP), 2,6-difluoropyridine (2,6-DFP), 3,5-difluoropyridine (3,5-DFP), 3,4,5-trifluoropyridine (3,4,5-TFP) and 2,4,6-trifluoropyridine (2,4,6-TFP), and pentafluoropyridine (PFP). Also, since we had previously investigated $CH_3CN–HCl$ and $H_3N–HCl$ using M06/aug-cc-pVTZ calculations, and that choice of method was based on a validation process (31), we initiated this work using that level of theory here as well.

However, we did encounter some complications in these initial, M06/aug-cc-pVTZ optimizations. Specifically, we had presumed a linear Cl-H--N interaction, which translates to C_{2v} symmetry for most complexes (2FP–HCl and 3FP-HCl being the exceptions). However, we found that the in-plane HCl wagging frequency was imaginary for all these C_{2v}-optimzed structures. A further tightening of the convergence criteria (from "opt=tight" to "opt=verytight") did not remedy this situation. We then fully relaxed the symmetry, and the result was that the N--H-Cl linkage bent significantly, essentially in the plane of the pyridine ring, by roughly 15° for most complexes. We had initially suspected that this was the result of an attractive interaction between the Cl and the hydrogen on the α-carbon of the pyridine ring, but the bend was even observed the systems with forward-facing fluorines in the 2- and 6-posiitons, though only 2-3°. After obtaining a full set of M06/aug-cc-pVTZ geometries within the C_s point group, all of which were bent along the N-H-Cl linkage but had real in-plane bending frequencies, we explored two additional methods; as a consistency check, and also to identify which best matched the experimental structure (36). These included both ωB97X-D, which has been optimal in some of our recent studies of Lewis acid-base systems (48, 49), as well as MP2, which offered an accessible post-Hartree-Fock method for comparison (the aug-cc-pVTZ basis set was used in both cases). What we

found for both ωB97X-D and MP2 was that the N-H-Cl linkage straightened; the C_s-symmetry, M06

starting structures became very nearly C_{2v} during the optimizations. Moreover, when these

optimizations were conducted within C_{2v}, the in-plane N-H-Cl bending frequencies were real, and the

energies of these structures (all obtained with the "verytight" setting) were found to be isoenergetic with

those with obtained in the absence of symmetry (±0.004 kcal/mol). Thus, we chose to report the results

obtained within the C_{2v} point group, even for the M06 binding energies. These are all about 0.2 kcal/mol

smaller in magnitude than the (equilibrium) bent, C_s structures, but the binding energy comparisons

across the three methods is more direct with a set of congruent structures. Ultimately, we found that

ωB897X-D/aug-cc-pVTZ best reproduced the measured N--Cl distance of C_5H_5N–HCl (2.999(5) Å) (36);

the ωB897X-D, M06 and MP2 results were 2.987 Å, 3.091 Å (3.085 Å in C_{2v}), and 3.195 Å, respectively.

In addition, ωB897X-D/aug-cc-pVTZ binding energy for C_5H_5N–HCl (10.2 kcal/mol), was most

consistent with the CCSD/aug-cc-pVTZ value (10.0 kcal/mol). For reference, the (C_{2v}) M06 and MP2

values were 8.7 and 11.0 kcal/mol, respectively. Overall, these results are significantly more accurate

than in an earlier MP2 study (16).

The ωB897X-D/aug-cc-pVTZ geometries for PYR–HCl and its singly-fluorinated analogs are

displayed in Figure 7, and a comparison of equilibrium N--H distances and binding energies from all

three methods (ωB97X-D, M06, and MP2) is presented in Table 1. As-a-whole, the ωB97X-D results

are intermediate between the other two methods, and overall, these results agree with the overall

experimental structural assessment for C_5H_5N–HCl (36). That is, beyond the agreement with measured

N--Cl distance, the stretching force constants and N nuclear quadrupole coupling constants depict a

system with a strong hydrogen bond with at most only a small extent of proton transfer (36). This is also

consistent with a previous energy decomposition analysis (16). Indeed, the N-H distance is rather short,

and the binding energy is substantial for an H-bonded system, exceeding that of H_3N–HCl (31). In turn,

the HCl bond elongates significantly due to this interaction, from 1.280 Å in free HCl to 1.362 Å in the

complex (ωB97X-D values), and the calculated (NPA) negative charge on the Cl increases in

magnitude (from -0.26e in free HCl to -0.41 I the complex). However, these changes fall well short of

those that seem to signal a significant degree of proton transfer (*see below*).

Figure 7: Equilibrium structures and binding energies for C_5H_5N–HCl and its singly fluorinated analogs at the ωB97X-D/aug-cc-pVTZ level of theory. Interatomic distances are displayed in units of Å. Charges on the chlorine atoms were obtained from Natural Population Analyses, and are included in parentheses (in units of e).

2
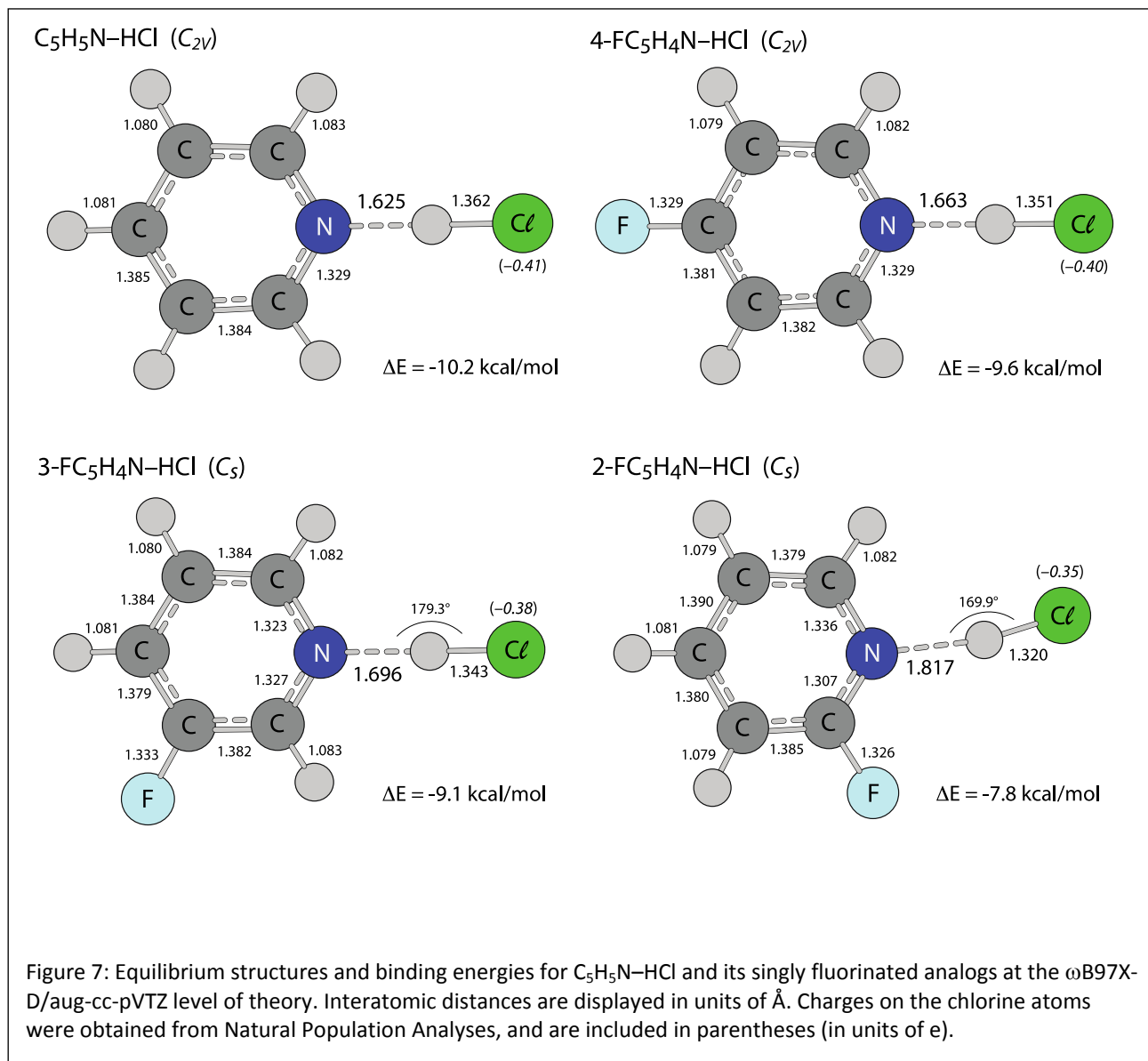
Table 1: N-H Distances and Binding Energies for C_5H_5N–HCl and various fluorinated analogs.

Method[a]	M06[b]		ωB97X-D		MP2	
Complex \ Property	R_{NH}[c]	ΔE[d]	R_{NH}[c]	ΔE[d]	R_{NH}[c]	ΔE[d]
C_5H_5N–HCl	1.749	-8.7	1.625	-10.2	1.618	-11
2-FC_5H_4N–HCl	1.880	-7.1	1.817	-7.8	1.787	-8.7
3-FC_5H_4N–HCl	1.803	-8.1	1.696	-9.1	1.672	-10.0
4-FC_5H_4N–HCl	1.773	-8.2	1.663	-9.6	1.654	-10.3
2,6-$F_2C_5H_3N$–HCl	1.986	-5.3	1.974	-5.9	1.942	-6.5
3,5-$F_2C_5H_3N$–HCl	1.835	-7.0	1.749	-8.2	1.713	-9.2
3,4,5-$F_3C_5H_2N$–HCl	1.845	-6.7	1.763	-7.8	1.732	-8.7
2,4,6-$F_3C_5H_2N$–HCl	1.996	-5.0	1.985	-5.6	1.954	-6.2
C_5F_5N–HCl	2.049	-3.8	2.054	-4.4	2.009	-5.1

a) With the aug-cc-pVTZ basis set. b) M06 values are for the C_{2v} structures (for the systems lacking fluorines in the 2- and 6-positions). c) True M06 minima are bent along the N--H-C linkage (Cs), and binding energies for the bent geometries are about 0.2 kcal/mol larger in magnitude. See text for discussion. d) Units of Å. e) Units of kcal/mol.

The singly fluorinated analogs are, as expected, correspondingly weaker, with longer N--H distances, and binding energies that are smaller in magnitude. However, as was noted previously (for di- and tri-substituted pyridines) (41, 42), substitution at the 2-poisiton has a more pronounced effect, and this will be discussed in more detail below, after the distinguishing features among these systems are noted. For 2FP–HCl, the N--H distance is 1.817 Å, nearly 0.2 Å longer than in PYR–HCl, and the binding energy is -7.8 kcal/mol, over 2 kcal/mol (nearly 25%) smaller than for PYR–HCl. For 4FP–HCl, the N--H distance is 1.663 Å, and the binding energy is -9.6 kcal/mol, which differ only slightly from the values for PYR–HCl. The results of 3FP–HCl are intermediate, but more closely resemble those of 4FP–HCl than 2FP–HCl. The trend in the Cl atomic charges also parallels this trend, and decreases (in magnitude) systematically, from -0.40e to -0.35e across the series of mono-fluoro complexes, in accord with the structure and binding energy results, and again, the value for 2FP–HCl is the most distinct.

2

The ωB97X-D/aug-cc-pVTZ structures for the di-, tri-, and penta-fluorinated complexes (2,6-DFP–HCl, 3,5-DFP–HCl, 2,4,6-TFP–HCl, 3,4,5-TFP–HCl, and PFP–HCl) are displayed in Figure 8. These results clearly illustrate the effect of further fluorination; not surprisingly, as the number of fluorines increases, the N--H distances increase, the binding energies decrease, and the charges on the Cl atoms become less negative. Again, we note that this general effect had been noted previously in an MP2 study (42). As a whole, these systems, together with those in Figure 7, illustrate the broad range of H-bonding strength that can be manifested via fluorine substitution on the pyridine ring. In the extreme, PFP–HCl is a complex has an N--H distance that is over 0.4 Å longer than in PYR–HCl, while the binding energy is 50% less. In fact, the complex is even weaker than CH_3CN–HCl (for which the M06/aug-cc-pVTZ binding energy is 6.0 kcal/mol) (31). The next weakest are the di- and tri-fluoro systems with the F's in the 2- and 6-positions (2,6-DFP–HCl and 2,4,6-TFP–HCl), and as a whole they are quite similar in terms of structure and overall strength. Here the N--H distances only 0.07 to 0.08 Å shorter than for PFP–HCl, and the binding energies are 1.2 to 1.5 kcal/mol larger. The remaining two systems, 2,6-DFP–HCl and 2,4,6-TFP–HCl, are comparable 2FP–HCl.
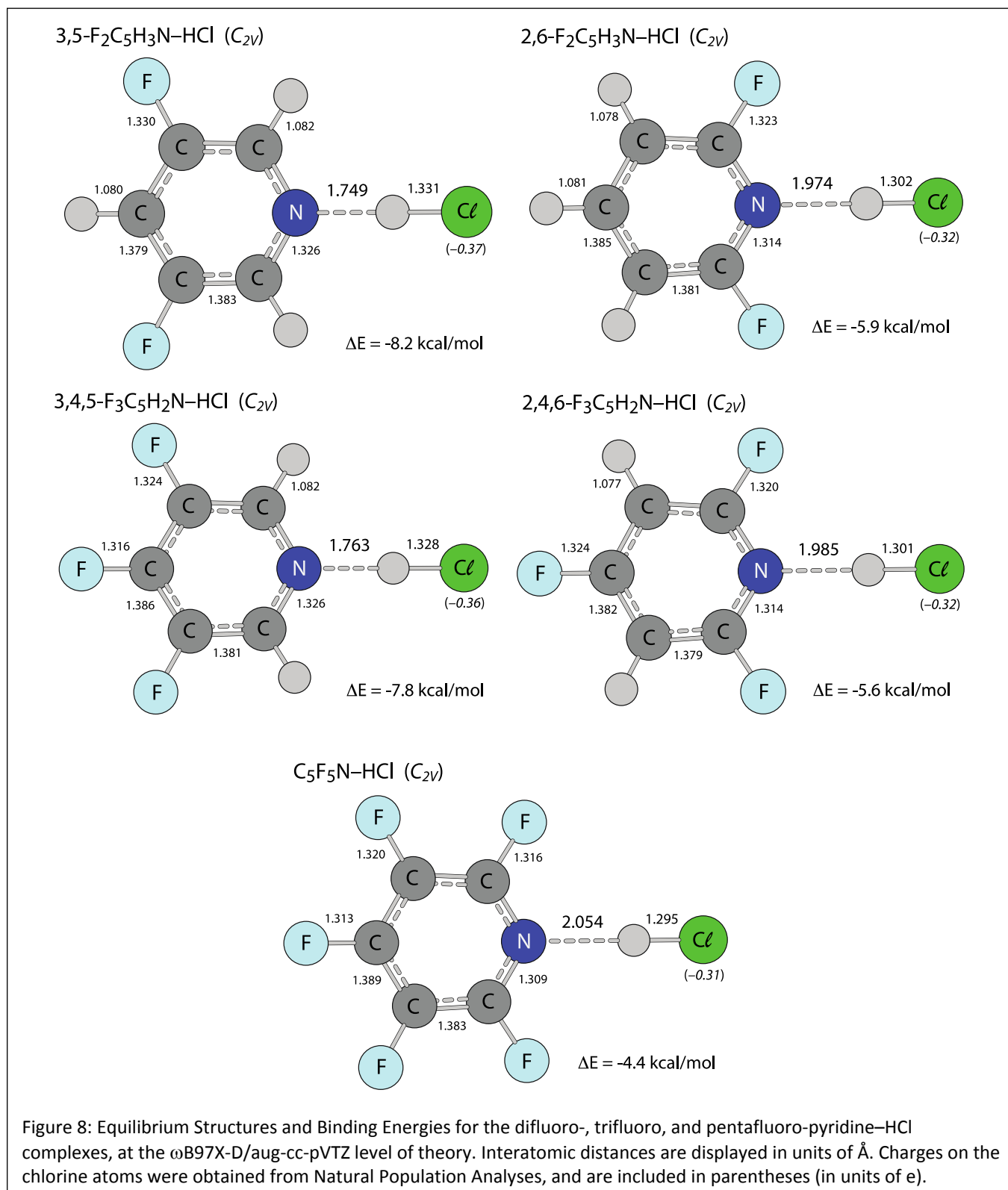
Figure 8: Equilibrium Structures and Binding Energies for the difluoro-, trifluoro, and pentafluoro-pyridine–HCl complexes, at the ωB97X-D/aug-cc-pVTZ level of theory. Interatomic distances are displayed in units of Å. Charges on the chlorine atoms were obtained from Natural Population Analyses, and are included in parentheses (in units of e).

The later comparison immediately above offers some insight as to the relative impact the subsequent fluorinations versus the position effect, and illustrates that fluorination at the 2- and 6-postions has the most pronounced, weakening influence on the base strength of the pyridine. Consider a comparison of 3FP–HCl to 3,5-DFP–HCl or 2FP–HCl; which illustrates a shift of a fluorine from 2-to-3, versus adding a second F at an equivalent position. Adding the second fluorine at the 5-position (*i.e.*, 3FP to 3,5-DFP), increases the N--H distance by 0.067 Å and the binding energy is reduced by 0.9 kcal/mol. Shifting the fluorine from 3-to-2 (*i.e.*, 3-FP to 2-FP) has a much more significant effect; the N--H distance increases by 0.12 Å, and the binding energy is reduced by 1.3 kcal/mol. Again, the 2FP-system, with a single fluorine in the adjacent position, has a nearly equal binding energy, and a longer N--H distance than in 3,4,5-TFP–HCl (*i.e.*, a trifluoro system lacking F's on the carbon adjacent to the N), but the bend along N--H-Cl suggests some degree electrostatic repulsion between the F and the Cl in 2FP–HCl. One other indicator of the position effect are the experimental results, specifically, the much larger red shift of the ν_{HCl} band for 3,5-DFP–HCl versus that of 2,6-DFP–HCl.

Interestingly, quantifying this effect via the computed charge distributions of the various fluoropyridines is less straightforward than we initially expected. In the earlier work on some of these systems, Sladek et al (41, 42), made some noteworthy observations, mostly based on the trends in the electrostatic potential surfaces. Specifically, they found that the regions near nitrogen atoms are by far the most negative portions of the various fluoropyridines, in spite of greater electronegativity of fluorine. In addition, they found that the extent of this region is muted to some extent with substitution at the 2- and 6-poitions, due to a region of positive potential at the corresponding carbons. Trends in the atomic charges are somewhat more perplexing, even those fit from the electrostatic potential in the earlier work (41, 42); for which the magnitude of the negative charge at the nitrogen is most greatly reduced by substitution at the 3-position (and specifically not the 2-postion).

2

The trends we calculated in the NPA charges for the pyridine nitrogens largely parallel those reported by Sladek et al, and moreover, the comparison of the mono-fluoropyrdines offers some additional clarity. The computed NPA charges on the N's for 2FP, 3FP, and 4FP are -0.46, -0.41, and -0.44 (units of e), respectively, and we note that for two of these, for 4FP and 2FP, are more negative than the value for PYR (-0.43). Initially, we had made the naïve assumption that fluorination would reduce the overall charge at the pyridine nitrogen, and that the shifts associated with position and the extent of fluorination would track with the strengths of the corresponding complexes (to some extent the charges derived from the electrostatic potential do track with extent (41, 42)). The nitrogen charges are distinctly less negative among the di- and tri- substituted systems, as well; the values for 2,6-DFP and 3,5-DFP are -0.49, and -0.39, respectively, while those for 2,4,6-TFP, and 3,4,5-TFP are -0.50 and -0.40, respectively. Even the NPA charge of the N in PFP (-0.47) is more negative than in pyridine. There is some rationale for these trends in the NPA charges, based in the "deactivating, orthro-para-directing" nature of F (*i.e.*, from the context of electrophilic aromatic substitution reactions). The upshot of such a characterization is that F-substitution would, overall, increase the negative charge in the ring ("deactivating"), and that this effect would be more pronounced at positions that are adjacent and opposite from the substitution site. Conversely, the substitution at meta sites, would be less pronounced, and for pyridine the 3-sites are meta to the nitrogen, resulting in less negative charge on the nitrogen for 3-F-pyrdines. Nonetheless, this consideration is based mainly on π electron density, and the hydrogen-bond acceptor site is a σ, sp^2-like, orbital, and thus the binding energies do not track well with the individual atomic charges. Perhaps, there is some degree of induction through the σ-framework that manifests the less-negative electrostatic potentials (41, 42) that do track with the binding energies. However, a repulsive, electrostatic interaction arising from the proximity of these α-fluorines to the binding HCl, could also be also significant contributor to this substituent effect, as has been suggested previously (37, 39, 40).

2

A comparison of predicted and observed frequency shifts seems warranted, in spite of the fact that

in our previous work (31) we did have some difficulty identifying computational methods that would

accurately predict the stretching frequency for HCl. Anharmonic corrections did improve the accuracy,

but then the predictions for the $CH_3CN–HCl$ complex predicted a red-shift that far exceed that of the

observed ν_{HCl} band in solid neon (31). Here we made some simplistic considerations based on a scale

factor and predicted red-shifts (*i.e.,* $\nu_{complex}$ - $\nu_{HCl(neon)}$). A scale factor of 0.967 was derived from the ratio

of the ωB79X-D/aug-cc-pVTZ prediction and measured gas-phase value for HCl (56). Applying this to

the predicted values for the complexes yielded frequency predictions which are somewhat *lower* than

the measured neon-matrix values, by 8, 24, and 32 cm^{-1}, for PFP–HCl, 2,6-DFP–HCl, and 3,5-DFP–

HCl, respectively. Comparing the predicted red-shifts lead to a similar result. For PFP–HCl, the

predicted ωB97X-D shift is -152 cm^{-1}, which is almost coincident what is observed in solid neon (-153

cm^{-1}; measured difference between ν_{HCl}(PFP–HCl) and ν_{HCl}(HCl)). For 2,6-DFP–HCl the predicted and

observed shifts are -312 and -273 cm^{-1}, respectively. For 3,5-DFP–HCl, these respective values are -

659 and -691 cm^{-1}. As with the scaling procedure, theory predicts gas-phase shifts that slightly exceed

the measured shifts in solid neon for the latter two systems. Thus, we have some degree of qualitative

agreement that lends some credibility to the frequency assignments and computational assessment.

On the other hand, with more reliable frequency predictions, one might expect the neon-matrix values

to lie just to the red of the gas-phase predictions (43, 57), consistent with a subtle matrix-effect on the

hydrogen bonds in these systems. This is not the case here, however.

Bonding Analyses and the Effects of Dielectric Media

In addition to the NPA charges that were discussed above in the context of the structures and

binding energies, we also conducted Atoms in in Molecules (AIM) analyses for a subset of these

systems. We chose these in an attempt to evenly span the overall range in binding energies, and avoid

redundancy in analyzing complexes of similar overall strength. This subset includes: PYR–HCl, 3-FP–

HCl, 3,5-DFP–HCl, 2,6-DFP-HCl, and PFP–HCl. Furthermore, we also investigated the effects of dielectric media on these systems via the Polarized Continuum Model (PCM), over a range of dielectric constants (1.2, 1.5, 2.0, 3.0, 5.0, 10.0, and 20.0), and examined the impact on structure as well as trends and bonding as revealed by NPA charges and AIM analyses. These, including the N--H and H-Cl distances, the NPA charge on the Cl, as well as the values for the density (ρ) and density Laplacian ($\nabla^2(\rho)$) for both the N-H and H-Cl bonds, are listed in Table 2. The gas-phase values ($\varepsilon=1.0$) are also included.

Table 2: Key Interatomic distances, and bonding parameters in the gas phase and dielectric media for C_5H_5N–HCl and select fluoro-analogs

C_5H_5N–HCl

ε	$R_{NH}{}^a$	$R_{HCl}{}^a$	$q_{Cl}{}^b$	$\rho_{NH}{}^c$	$\rho_{HCl}{}^c$	$\nabla^2(\rho)_{NH}{}^d$	$\nabla^2(\rho)_{HCl}{}^d$
1.0	1.625	1.362	-0.41	0.07	0.20	0.04	-0.58
1.2[e]	**1.489 /** **1.185**	**1.410 /** **1.631**	**-0.47 /** **-0.68**	**0.10 /** **0.21**	**0.18 /** **0.10**	**-0.02 /** **-0.77**	**-0.45 /** **-0.08**
1.5	1.136	1.570	-0.74	0.24	0.08	-1.13	-0.01
2.0	1.106	1.709	-0.79	0.26	0.07	-1.39	0.02
3.0	1.084	1.966	-0.83	0.28	0.06	-1.60	0.04
5.0	1.069	1.896	-0.86	0.29	0.05	-1.75	0.05
10.0	1.059	1.941	-0.88	0.30	0.05	-1.84	0.06
20.0	1.055	1.966	-0.89	0.31	0.05	-1.88	0.06

3-FC_5H_4N–HCl

ε	$R_{NH}{}^a$	$R_{HCl}{}^a$	$q_{Cl}{}^b$	$\rho_{NH}{}^c$	$\rho_{HCl}{}^c$	$\nabla^2(\rho)_{NH}{}^d$	$\nabla^2(\rho)_{HCl}{}^d$
1.0	1.696	1.343	-0.38	0.06	0.21	0.06	-0.64
1.2	1.650	1.355	-0.40	0.07	0.21	0.05	-0.60
1.5[e]	**1.553 /** **1.171**	**1.386 /** **1.653**	**-0.44 /** **-0.70**	**0.08 /** **0.22**	**0.192 /** **0.10**	**0.01 /** **-0.87**	**-0.52 /** **0.06**
2.0	1.125	1.733	-0.76	0.25	0.08	-1.22	0.00
3.0	1.097	1.803	-0.81	0.27	0.07	-1.49	0.03
5.0	1.078	1.862	-0.84	0.29	0.06	-1.66	0.04
10.0	1.067	1.908	-0.86	0.30	0.05	-1.77	0.05
20.0	1.062	1.933	-0.87	0.30	0.05	-1.82	0.06

3,5-F$_2$C$_5$H$_3$N–HCl

ε	R_{NH}[a]	R_{HCl}[a]	q_{Cl}[b]	ρ_{NH}[c]	ρ_{HCl}[c]	$\nabla^2(\rho)_{NH}$[d]	$\nabla^2(\rho)_{HCl}$[d]
1.0	1.749	1.331	-0.37	0.05	0.22	0.06	-0.67
1.2	1.715	1.338	-0.38	0.06	0.22	0.06	-0.65
1.5	1.670	1.349	-0.39	0.06	0.21	0.05	-0.62
2.0[e]	1.584 / **1.156**	1.375 / **1.679**	-0.43 / **-0.72**	0.08 / **0.22**	0.20 / **0.09**	0.03 / **-1.00**	-0.55 / **-0.04**
3.0	1.113	1.763	-0.78	0.26	0.07	-1.33	0.01
5.0	1.090	1.825	-0.82	0.28	0.06	-1.55	0.03
10.0	1.076	1.875	-0.85	0.29	0.06	-1.69	0.05
20.0	1.070	1.901	-0.86	0.29	0.05	-1.75	0.05

2,6-F$_2$C$_5$H$_3$N–HCl

ε	R_{NH}[a]	R_{HCl}[a]	q_{Cl}[b]	ρ_{NH}[c]	ρ_{HCl}[c]	$\nabla^2(\rho)_{NH}$[d]	$\nabla^2(\rho)_{HCl}$[d]
1.0	1.974	1.302	-0.32	0.03	0.24	0.07	-0.76
1.2	1.955	1.304	-0.33	0.03	0.24	0.07	-0.75
1.5	1.932	1.307	-0.33	0.03	0.24	0.07	-0.75
2.0	1.902	1.311	-0.34	0.03	0.23	0.07	-0.74
3.0	1.868	1.315	-0.35	0.04	0.23	0.07	-0.73
5.0	1.836	1.320	-0.36	0.04	0.23	0.07	-0.72
10.0	1.802	1.326	-0.37	0.04	0.22	0.07	-0.70
20.0	1.783	1.329	-0.38	0.05	0.22	0.07	-0.69

C$_5$F$_5$N–HCl

ε	R_{NH}[a]	R_{HCl}[a]	q_{Cl}[b]	ρ_{NH}[c]	ρ_{HCl}[c]	$\nabla^2(\rho)_{NH}$[d]	$\nabla^2(\rho)_{HCl}$[d]
1.0	2.054	1.295	-0.31	0.02	0.24	0.06	-0.77
1.2	2.036	1.296	-0.31	0.03	0.24	0.06	-0.77
1.5	2.016	1.298	-0.31	0.03	0.24	0.06	-0.77
2.0	1.994	1.300	-0.32	0.03	0.24	0.07	-0.76
3.0	1.969	1.303	-0.33	0.03	0.24	0.07	-0.76
5.0	1.946	1.305	-0.33	0.03	0.24	0.07	-0.75
10.0	1.925	1.308	-0.34	0.03	0.24	0.07	-0.75
20.0	1.911	1.310	-0.34	0.03	0.23	0.07	-0.74

a) Units of Å; Units of elementary charge (e). b) Units of a.u., equivalent to electrons/bohr^3. c) Units of a.u., equivalent to electrons/bohr^5. e) Two minimum-energy structures were located for these ε-values. Data for the global minima are in bold, and these structures are 0.3-0.5 kcal/mol lower in energy than their metastable counterparts. See text for discussion.

2

The trends in the AIM parameters for the gas-phase systems very much parallel the observed trends in the structure and binding energy, and do indicate some degree of electron rearrangement, especially for the stronger systems. For one, we note that bond critical points (BCP's) were located along the N--H bond path in these systems, as is expected for hydrogen bonding interactions (8, 11, 58, 59). A typical range quoted for these density values is 0.002 to 0.040 a.u. (*i.e.*, electrons/bohr^3) (11, 58). In one study involving a representative sample of complexes with O-H, F-H, N-H, and HCl donors, this range extends to 0.6 a.u., and the value for H_3N–HCl lies near this extreme (14). For some exceptionally strong hydrogen bonds, with significant covalent character, this value can approach the ~0.1 a.u., the stated threshold for shared (*i.e.*, covalent) interactions (11, 13, 59). For PYR–HCl, the value of the density at the N--H bond critical point (ρ_{NH}) is 0.07 a.u., which lies beyond the upper limit for the typical hydrogen-bond range, just beyond the H_3N–HCl value (14). For additional context, we note that the ρ-value at the H-bond critical points for water dimer is 0.02 a.u., respectively. The upshot is that the hydrogen bond in PYR–HCl lies right at the threshold in which covalent contributions become significant, and as we will see below, this system is on the verge of proton transfer as well. As expected, the ρ_{NH} values decrease with fluorination, ranging from 0.06 a.u. for 3FP–HCl to 0.02 a.u. for PFP–HCl, and only the two weakest systems, 2,6-DFP and PFP–HCl lie within the "typical" range quoted above. Overall, these systems exhibit relatively large values for the electron density at the BCP, especially in the case of the stronger systems in the series, which approach values consistent with significant covalent charter in the interaction.

Trends in the values of the Laplacian at the N--H critical points ($\nabla^2(\rho)_{NH}$) parallel those for the densities. In general, $\nabla^2(\rho)$ values are positive for "ionic" (closed-shell) interactions, and negative for "shared" (covalent) interactions (51), and the typical range quoted for hydrogen bonds is about +0.02 to +0.15 a.u. (*i.e.*, electrons/bohr^5) (11, 13, 14, 59). Here, the smaller values correspond to stronger systems, and the values can be negative for exceptionally strong systems with significant covalent

character (11). For PYR–HCl, the $\nabla^2(\rho)_{NH}$ value is 0.04 a.u., near the lower limit of the "typical" range. With fluorination, the $\nabla^2(\rho)_{NH}$ values increase somewhat, from 0.06 a.u. for 3FP-HCl to 0.07 a.u. for 2,6-DFP–HCl (which is a bit larger than the value for PFP-HCl). Here, the range of values lies within the stated range for hydrogen bonding, near the limit corresponding to stronger interactions.

The topological properties of the H-Cl bonds, ρ_{HCl} and $\nabla^2(\rho)_{HCl}$ also vary systematically with the strength of the complexes, and do convey a sequential degree of electron rearrangement with the HCl subunit. The ρ_{HCl} value for free HCl is 0.25 au, and the values in the complexes vary from 0.21 a.u. for PYR–HCl to 0.24 a.u. for PFP–HCl, indicating a slight loss of electron density in the HCl bond, even at the weak end of the series. Meanwhile, the $\nabla^2(\rho)_{HCl}$ values, which are fairly large and negative (typical of covalent bonds) (51), and tend to increase in magnitude with fluorination; the value for PYR–HCl is -0.58 a.u., while the value for PFP–HCl is -0.74 units (free HCl is -0.80 a.u.). This trend indicates a subtle shift towards ionic character between PFP–HCl and PYR-HCl.

When we investigated these systems in bulk dielectric media, we observed is a distinct transition to Type III (H$^+$-transfer) complexes at relatively low ε-values for PYR-HCl, 3FP–HCl, and 3,5-DFP–HCl. This is signaled by a lengthening of the H-Cl bond (from 1.3 to 1.6-1.8 Å), a shortening of the N-H bond (from 1.6-1.7 Å to 1.1 Å), and an increase in the negative charge of the Cl (from -0.4e to -0.8e or more). This transition takes place at slightly higher dielectrics as the complex is weakened by fluorine substitution, occurring at about ε=1.2 for PYR–HCl, ε=1.5 for 3FP–HCl, and ε=2.0 for 2,6-DFP–HCl. Moreover, at each of these, "transitional" dielectrics, there are two stable minima. The meta-stable (Type I) minima we located while performing successive optimizations with increasing ε-values, while the global (Type III) minima were located performing successive optimizations while decreasing the ε-value. We were aware of a proton-transfer barrier for some of these systems due to in-progress studies of their intermolecular potentials, and thus opted to scan the dialectic in both directions to ensure we

3

located the global minima (bold in Table 2), which lie 0.3 to 0.5 kcal/mol below the metastable Type-I

minima. The upshot is that as the dielectric is increased, the transition to the Type-III structure takes

place (*i.e.*, ε=1.5 for PYR–HCl) when the barrier disappears, not necessarily when the ion-pair structure

becomes more energetically stable (*i.e.*, ε=1.2 for PYR–HCl). Also, we note that we only located

secondary minima at a single, transitional dielectric value for each system; no metastable structures

were identified at other ε-values. In addition, we emphasize that the transition to stable Type III

structures is largely distinct; identified no stable structures that would be aptly described as "proton

shared" (Type II).

The transition to Type-III complexes does not take place for 2,6-DFP–HCl and PFP–HCl; these

systems persist as Type-I, hydrogen-bonded structures throughout the dielectrics we sampled.

However, the hydrogen bonds are strengthened by the media, as evidenced by slightly compressed N-

H distances and elongated H-Cl distances, as well as a marginal increase in the negative charge on the

chlorine. This is remarkably consistent with our experimental matrix-IR results for these systems. In

turn, the fact that the medium response for 3,5-DFP–HCl is predicted to manifest proton transfer, is

consistent, at least in a general sense, with the larger shift and marked broadening for the ν_{HCl} band in

those spectra. However, we predict that the effect would not take place until ε=2.0, which is beyond the

dielectric constants estimated for these matrix media (60). Nevertheless, we note also that the theory

results reflect the equilibrium geometries, and if the proton-transfer barriers are low, dynamical

averaging along the proton-stretching coordinate would manifest experimental signatures of a Type-II

or III structure at lower ε-values than theory would predict (see below).

This consideration may also apply to how these data compare to previous work on PYR–HCl and its

4-substities analogs (37-40). The reasonably distinct Type I-to-Type III transition for the stronger

systems would seem to suggest that barriers along the proton-transfer coordinates preclude the

existence of any proton-shared, Type-II structures. However, we did not attempt to fine-tune the

dielectric values in an attempt to identify such structures, and some of the data for the metastable structures at the transitional dielectrics look somewhat intermediate (*e.g.*, PYR–HCl for ε=1.2). Regardless, the absence of stable Type-II structures would seem to conflict with what has been observed in experimental matrix IR spectra for PYR-HCl and several of its 4-substitied analogs (37-40), which seem to convey proton-sharing. Pending a thorough analysis of the intermolecular potential surfaces of these systems (which is in progress), we suspect that the proton transfer barriers are small, such the that the ground-state vibrational amplitude of the hydrogen atom encompasses both the hydrogen bond (Type I) and proton transfer (Type III) regions of the potential. We do note that this was situation that prior investigations noted for PYR–HCl. In both the empirically derived (37) and ab initio (MP2) potentials (38), the proton stretching amplitude encompasses the hydrogen-bonding and proton-transfer structures. Why a proton transfer barrier persists in PYR–HCl and its analogs, but is not present for H_3N–HCl (61), is yet another interesting and unresolved question, however.

The trends in the topological properties also reflect the enhancement of the hydrogen bonds in the dielectric media, and exhibit dramatic shifts that signal clear changes in the bonding when proton transfer occurs. As the dielectric is increased, prior to H^+ transfer for PYR–HCl, 3FP–HCl, and 3,5-DFP-HCl, or throughout the data for 2,6-DFP–HCl or PFP–HCl, the ρ_{NH} values increase as the H-bonds are strengthened by the dielectric media. Conversely, the ρ_{HCl} values tend to stay reasonably constant over these ranges, with only a slight decrease at the extremes of the 2,6-DFP–HCl and PFP–HCl data, Interestingly, there seems to be a signal of the onset of proton transfer in the ρ_{NH} values, which reach an apparent threshold of about 0.08 a.u., immediately prior to proton transfer, and the systems that do not undergo such a transition never reach that value. This is essentially a quantification of the conceptual idea stated by Grabowski in his recent review (13); that there must be some degree of covalency in the hydrogen bond in order for proton transfer to take place. Here, the observed threshold lies somewhat below the stated 0.1 a.u. for significant covalent character (11, 13, 59), however.

3

As for the Laplacians, the $\nabla^2(\rho)_{HCl}$ values steadily decrease in magnitude as the H-bond strength is enhanced by the media, which is consistent with a shift towards more ionic character. The values decrease to threshold of about 0.05 a.u. near the onset of proton transfer, after which they become negative. The exceptions are the metastable structures at the transition points for PYR–HCl, 3FP–HCl, and 3,5-DFP-HCl. This apparent threshold value is never reached for 2,6-DFP–HCl and PFP–HCl; the $\nabla^2(\rho)_{NH}$ values are consistent (0.06 to 0.07 a.u.) throughout the range of dielectrics examined. Overall, it is clear that the trends in the AIM data reveal internal shifts in the electron density that seem to take place as the H-bonds are strengthen, either by via media or via the extent of fluorination on the pyridine ring, and may in some instances signal the onset of proton transfer.

The AIM parameters for the Type-III structures of PYR–HCl, 3FP–HCl, and 3,5-DFP-HCl illustrate distinct differences in bonding relative to the Type-I structures, and also indicate continuing changes that take place beyond the initial onset of proton transfer. One key difference is in the ρ values; the ρ_{NH} values are increase abruptly from ~0.08 a.u. to ~0.25 a.u. upon proton transfer, and then continue to increase at higher dielectric values. Conversely, the ρ_{HCl} values are decrease from ~0.2 a.u. to ~0.08 a.u. after proton transfer, and then continue to decrease at higher dielectric values. An analogous trend is apparent in the Laplacian data. The $\nabla^2(\rho)_{HCl}$ values transition from fairly large and negative, to small and positive, while the $\nabla^2(\rho)_{NH}$ values trend in the opposite manner. These shifts are consistent with shifts to a covalent N-H bond, and an ionic H--Cl bond. To a small extent, the trends in the $\nabla^2(\rho)$ values continue toward high dielectrics, and thus indicate that some additional shifting in the electron density continues to take place, even after the more abrupt changes that mark the onset proton transfer.

There is also a rather interesting consistency in these data; the sums of the ρ_{NH} and ρ_{HCl} values are nearly constant among each type of structure. For the Type-I structures the sum of the ρ_{NH} and ρ_{HCl} values is about 0.27 a.u.; not only across all the gas-phase structures in the subset, but also among

3

those in the dialectic media for which proton transfer has not yet occurred. This value is just a bit larger than the vale for free HCl (0.25 a.u.). That is, as the H-bonds are enhanced (via intermolecular or intramolecular factors), the increase in density in the N--H hydrogen bond is matched by a corresponding decrease in density in the H-Cl bond. To some extent, this mimics the "conservation of bond order" principle outlined in the recent review by Grabowski (13) using solid-state structural data for a series of compounds with intramolecular O--H-O hydrogen bonds with varying degrees of strength and/or proton transfer. Across this series, the sum of the empirically-defined (*i.e.*, on the basis of distance) bond orders for the two O-H bonds remains constant, even as the individual values vary with the interaction strength. Here, there seems to be a corresponding trend in the density values among the hydrogen-bonded structures, but it does not necessarily extend to the Type-III, proton-transfer structures. There is a nearly constant value for the sum of ρ_{NH} and ρ_{HCl} among those structures as well, but the values (about 0.33) somewhat exceed those for the Type-I structures. This is inconsistent with the basic idea of bond order conservation, which is shown to apply across the proton-transfer transition with empirically defined bond orders. Perhaps this is due to the proton transfer barrier in this system, which renders these Type I and Type III structures distinct. Regardless, a survey of existing AIM data on analogous systems is certainly warranted, which would reveal the extent to whether such observations occur in any widespread sense.

Conclusions

We have conducted an extensive experimental and theoretical investigation of pyridine-HCl and several of its fluorinated analogs. Matrix IR spectra of pentafluoropyridine-HCl, 2,6-difluoropyridine–HCl, and 3,5-difluoropyridine–HCl reveal systematic red-shifts in the ν_{HCl} bands that convey both substituent effects and matrix effects on hydrogen-bond strength. The observed neon matrix frequencies (3,5-PFP-HCl < 2,6-DFP–HCl < PFP–HCl) shift to lower frequencies with increasing fluorination and/or substitution at the carbons adjacent to the nitrogen. In addition, the spectra for

3

pentafluoropyridine-HCl, and 2,6-difluoropyridine–HCl show significant matrix shifts for the ν_{HCl} bands

(N_2 < Ar < Ne), especially in the latter instance, which indicate a systematic enhancement of the

hydrogen bonds, which parallels the "solvent" stabilization of the hosts.

We also conducted a computational study of pyridine-HCl and eight fluorinated analogs. Structures

and binding energies indicate that, overall, the interactions in this set of complexes span a broad range

of moderately strong hydrogen bonds. This is apparent not only in the binding energy values (which

range from 4.4 to 10.2 kcal/mol via wB97X-D/aug-cc-pVTZ), but also in the trends in the N-H and H-Cl

distances, and calculated (NPA) charges on chlorines. The effect of fluorine substitution is systematic

and shows two clear trends. With increasing fluorination, the hydrogen bonds weaken, and in turn, the

N-H distances increase, the H-Cl distances decrease, and the magnitude of the charge on Cl

decreases. In addition, we found, as in previous work (41, 42), that fluorine substitution at the 2- and 6-

positions has a more pronounced effect than substitution at other sites on the pyridine ring.

Interestingly, the strengths of the complexes do not directly parallel fluorine-induced trends in the

computed atomic charges of the pyridine nitrogen, and suggests that the effect of fluorine substitution

on the pyridine ring is a more complicated matter than simple induction.

Bonding analyses for the gas-phase complexes reveal shifts in the electron density that parallel that

variations in strength that result from fluorine substitution. Values of the electron density at the

hydrogen bond critical points (ρ_{NH}) for the stronger members of this set significantly exceed these

stated for typical hydrogen bonds, and across the series, the values systematically decrease with

fluorination. The corollary effect on the ρ_{HCl} values is more subtle, these are less than that for free HCl,

and do decrease as with hydrogen bond strength increases (*i.e.*, increase with fluorination). Values for

density Laplacians ($\nabla^2(\rho)$) at the H-Cl and N--H bond critical points also shift somewhat among the gas-

phase structures. As the interaction energy increases, these ($\nabla^2(\rho)$) values suggest a mild increase in

covalent character for the N--H bond and a corresponding increase in ionic character for the H-Cl bond.

3

For several of the complexes, pyridine-HCl, 3-flurorpyridine–HCl, and 3,5-diflurorpyrdine–HCl, we predict a transition to Type-III proton-transfer type structures in low-dielectric media, at ε-values of 1.2, 1.5, and 2,0 respectively. This transition is signaled a substantial shortening of N-H distance, a lengthening of the H-Cl distance, and an increase in the negative charge on the chlorine. Moreover, there are parallel increases and decreases in the ρ_{NH} and ρ_{HCl} values respectively, the $\nabla^2(r)$ values depict a switch to a covalent N-H bond, and an ionic H-Cl bond. Conversely, we see no indication of proton transfer in dielectric media for 2,6-difluropyridine–HCl, and pentafluoropyridine–HCl, but the predicted structural and bonding properties do depict a systematic strengthening of the hydrogen bonding in these systems, and are quite consistent with the experimental IR spectra.

Conflict of interest statement
There are no conflicts to declare.

Author Contributions

Soares: Investigation, Data Curation, Formal Analysis, Writing – original draft.

Ley: Investigation, Data collection.

Zehner: Investigation, Data collection.

Treacy: Investigation, Data collection.

Phillips: Conceptualization, Funding Acquisition, Methodology, Project Administration, Supervision, Writing – review and editing

References

1. Pimentel GG, McClellan AL. The Hydrogen Bond. San Francisco, CA: W. H. Freeman & Co.; 1960.

2. Jeffrey GA. An Introduction to Hydrogen Bonding: Oxford University Press; 1997.

3. Grabowski S. Hydrogen Bonding - New Insights: Springer Netherlands; 2013.

4. Grabowski SJ. Understanding Hydrogen Bonds: Theoretical and Experimental Views: Royal Society of Chemistry; 2020.

5. Pimentel GC, McClella.Al. HYDROGEN BONDING. Annual Review of Physical Chemistry. 1971;22:34.

6. Emsley J. VERY STRONG HYDROGEN-BONDING. Chemical Society Reviews. 1980;9(1):91-124.

7. Perrin CL, Nielson JB. "Strong" hydrogen bonds in chemistry and biology. Annual Review of Physical Chemistry. 1997;48:511-44.

8. Grabowski SJ. Hydrogen bonding strength - measures based on geometric and topological parameters. Journal of Physical Organic Chemistry. 2004;17(1):18-31.

9. Pak C, Lee HM, Kim JC, Kim D, Kim KS. Theoretical investigation of normal to strong hydrogen bonds. Structural Chemistry. 2005;16(3):187-202.

10. Pendas AM, Blanco MA, Francisco E. The nature of the hydrogen bond: A synthesis from the interacting quantum atoms picture. Journal of Chemical Physics. 2006;125(18).

11. Grabowski SJ. What Is the Covalency of Hydrogen Bonding? Chemical Reviews. 2011;111(4):2597-625.

12. Jablonski M. A Critical Overview of Current Theoretical Methods of Estimating the Energy of Intramolecular Interactions. Molecules. 2020;25(23).

13. Grabowski SJ. Hydrogen Bond and Other Lewis Acid-Lewis Base Interactions as Preliminary Stages of Chemical Reactions. Molecules. 2020;25(20).

14. Poater J, Fradera X, Sola M, Duran M, Simon S. On the electron-pair nature of the hydrogen bond in the framework of the atoms in molecules theory. Chemical Physics Letters. 2003;369(1-2):248-55.

15. Poater J, Sola M, Bickelhaupt FM. A model of the chemical bond must be rooted in quantum mechanics, provide insight, and possess predictive power. Chemistry-a European Journal. 2006;12(10):2902-5.

16. Wu JY, Yan H, Jin YX, Dai GL, Zhong AG. Characteristics and nature of the intermolecular interactions between pyridine and various hydrides: A theoretical study. Journal of Molecular Structure-Theochem. 2010;944(1-3):70-5.

17. Su PF, Tang Z, Wu W. Generalized Kohn-Sham energy decomposition analysis and its applications. Wiley Interdisciplinary Reviews-Computational Molecular Science. 2020;10(5).

18. Poater J, Swart M, Guerra CF, Bickelhaupt FM. Solvent effects on hydrogen bonds in Watson-Crick, mismatched, and modified DNA base pairs. Computational and Theoretical Chemistry. 2012;998:57-63.

19. Fedorov DG, Kitaura K. Pair interaction energy decomposition analysis. Journal of Computational Chemistry. 2007;28(1):222-37.

20. Dereka B, Yu Q, Lewis NHC, Carpenter WB, Bowman JM, Tokmakoff A. Crossover from hydrogen to chemical bonding. Science. 2021;371(6525):160-+.

21. Ault BS, Steinback E, Pimentel GC. Matrix-Isolation Studies of Hydrogen Bonding - Vibrational Correlation Diagram. Journal of Physical Chemistry. 1975;79(6):615-20.

22. Legon AC. The nature of the Ammonium and Methylammonium Halides in the Vaopr Phase - Hydrogen Bonding versus Proton Transfer. Chemical Society Reviews. 1993;22(3):153-63.

23. Barnes AJ, Legon AC. Proton transfer in amine-hydrogen halide complexes: comparison of low temperature matrices with the gas phase. Journal of Molecular Structure. 1998;448(2-3):101-6.

24. Brauer CS, Craddock MB, Kilian J, Grumstrup EM, Orilall MC, Mo YR, et al. Amine-hydrogen halide complexes: Experimental electric dipole moments and a theoretical decomposition of dipole moments and binding energies. Journal of Physical Chemistry A. 2006;110(33):10025-34.

25. Ault BS, Pimentel GC. Infrared Spectra of the Ammonia-Hydrochloric Acid Complex in Solid Nitrogen. Journal of Physical Chemistry. 1973;77(13):1649-53.

26. Barnes AJ, Beech TR, Mielke Z. Strongly Hydrogen Bonded Molcular Complexes Studied by Matrix-Isolation Vobrational Spectroscopy. 1. The Ammonia Hydrogen Chloride Complex. Journal of the Chemical Society-Faraday Transactions Ii. 1984;80:455-63.

27. Goodwin EJ, Howard NW, Legon AC. The Rotaitonal Spectrum of N-15 Ammonium Chloride Vapor-Characterization of the Hydrogen-Bonded Dimer $H_3N..HCl$. Chemical Physics Letters. 1986;131(4-5):319-24.

28. Howard NW, Legon AC. ature, Geometry, and Binding Strength of the Ammonia-Hydrogen Chloride Dimer Determined from the Rotational Spectrum of Ammonium Chloride Vapor. Journal of Chemical Physics. 1988;88(8):4694-701.

29. Andrews L, Wang XF, Mielke Z. Infrared spectrum of the H_3N-HCl complex in solid neon. Journal of the American Chemical Society. 2001;123(7):1499-500.

30. Andrews L, Wang XF, Mielke Z. Infrared spectrum of the H_3N-HCl complex in solid Ne, Ne/Ar, Ar, and Kr. Matrix effects on a strong hydrogen-bonded complex. Journal of Physical Chemistry A. 2001;105(25):6054-64.

31. Weiss NM, Waller AW, Phillips JA. Infrared spectrum of CH_3CN-HCl in solid neon, and modeling matrix effects in CH_3CN-HCl and H_3N-HCl. Journal of Molecular Structure. 2016;1105:341-9.

32. Avakyan VG, Golitsyna TL, Kimelfeld YM. Structure of the Complexes of HCl with Pyrdine and Trimethyl Amine, Isolated in and Ar Matrix. Journal of Structural Chemistry. Journal of Structural Chemistry. 1978;19(6):877-82.

33. Barnes AJ, Szczepaniak K, Orvillethomas WJ. Study of Intermolecular interactions by Matrix-Isolation Vobrarional Spectroscopy. Journal of Molecular Structure. 1980;59(JAN):39-53.

34. Jordan MJT, Del Bene JE. Unraveling environmental effects on hydrogen-bonded complexes: Matrix effects on the structures and proton-stretching frequencies of hydrogen-halide complexes with ammonia and trimethylamine. Journal of the American Chemical Society. 2000;122(9):2101-15.

35. Hamlin TA, Poater J, Guerra CF, Bickelhaupt FM. B-DNA model systems in non-terran bio-solvents: implications for structure, stability and replication. Physical Chemistry Chemical Physics. 2017;19(26):16969-78.

36. Cooke SA, Corlett GK, Lister DG, Legon AC. Is pyridinium hydrochloride a simple hydrogen-bonded complex C5H5N center dot center dot center dot HCl or an ion pair C5H5NH+center dot center dot center dot Cl- in the gas phase? An answer from its rotational spectrum. Journal of the Chemical Society-Faraday Transactions. 1998;94(7):837-41.

37. Szczepaniak K, Chabrier P, Person WB, Del Bene JE. Experimental infrared spectra of matrix isolated complexes of HCl with 4-substituted pyridines. Evaluation of anharmonicity and matrix effects using data from ab initio calculations. Journal of Molecular Structure. 2000;520:1-18.

38. Chapman K, Crittenden D, Bevitt J, Jordan MJT, Del Bene JE. Relating environmental effects and structures, IR, and NMR properties of hydrogen-bonded complexes: ClH : pyridine. Journal of Physical Chemistry A. 2001;105(22):5442-9.

39. Delbene JE, Person WB, Szczepaniak K. Ab Initio Theroetical and Matrix-Isolation Experimental Studies of Hydrogen-Bonding - Vibrational Consequences of Proton Position in 1/1 Complexes of HCl AND 4-X-Pyridines. Chemical Physics Letters. 1995;247(1-2):89-94.

40. DelBene JE, Person WB, Szczepaniak K. Ab initio theoretical and matrix isolation experimental studies of hydrogen bonding .2. A theoretical study of distances, force constants, and vibrational frequencies in complexes of hydrogen halides and 4-substituted pyridines. Molecular Physics. 1996;89(1):47-59.

41. Sladek V, Punyain K, Ilcin M, Lukes V. Substitution Effect on the Intermolecular Halogen and Hydrogen Bonds of the r-Bonded Fluorinated Pyridine...XY/HX Complexes (XY=F_2, Cl_2, ClF; HX=HF, HCl). International Journal of Quantum Chemistry. 2014;114(13):869-78.

42. Sladek V, Skorna P, Poliak P, Lukes V. The ab initio study of halogen and hydrogen sigma(N)-bonded para-substituted pyridine ... (X-2/XY/HX) complexes. Chemical Physics Letters. 2015;619:7-13.

43. Eigner AA, Rohde JA, Knutson CC, Phillips JA. IR spectrum of CH_3CN-BF_3 in solid neon: Matrix effects on the structure of a Lewis acid-base complex. Journal of Physical Chemistry B. 2007;111(6):1402-7.

44. M. J. Frisch GWT, H. B. Schlegel, G. E. Scuseria, M. A. Robb JRC, G. Scalmani, V. Barone, B. Mennucci, G. A. Petersson HN, M. Caricato, X. Li, H. P. Hratchian, A. F. Izmaylov JB, G. Zheng, J. L. Sonnenberg, M. Hada, M. Ehara KT, R. Fukuda, J. Hasegawa, M. Ishida, T. Nakajima, Y. Honda OK, H. Nakai, T. Vreven, J. A. Montgomery, Jr., et al. Gaussian 09, Revision B.01. Wallingford CT: Gaussian, Inc.; 2010.

45. Zhao Y, Truhlar DG. The M06 suite of density functionals for main group thermochemistry, thermochemical kinetics, noncovalent interactions, excited states, and transition elements: two new

3

functionals and systematic testing of four M06-class functionals and 12 other functionals. Theoretical Chemistry Accounts. 2008;120(1-3):215-41.

46. Chai JD, Head-Gordon M. Long-range corrected hybrid density functionals with damped atom-atom dispersion corrections. Physical Chemistry Chemical Physics. 2008;10(44):6615-20.

47. Cramer CJ. Essentials of computational chemistry: theories and models: Wiley. com; 2005.

48. Helminiak HM, Knauf RR, Danforth SJ, Phillips JA. Structural and Energetic Properties of Acetonitrile-Group IV (A & B) Halide Complexes. Journal of Physical Chemistry A. 2014;118(24):4266-77.

49. Munos JA, Lowney DT, Phillips JA. Structural and energetic properties of OC-BX3 complexes: unrealized potential for bond-stretch isomerism. Physical Chemistry Chemical Physics. 2021;23(27):14678-86.

50. Reed AE, Weinstock RB, Weinhold F. Natural population analysis. Journal of Chemical Physics. 1985;83(2):735-46.

51. Bader RFW. Atoms in Molecules. Accounts of Chemical Research. 1985;18(1):9-15.
52. Tomasi J. Thirty years of continuum solvation chemistry: a review, and prospects for the near future. Theoretical Chemistry Accounts. 2004;112(4):184-203.

53. Dunkin I. Matrix Isolation Techniques: A Practical Approach. Oxford, UK: Oxford University Press; 1998.

54. NIST Chemistry Webbook: http://webbook.nist.gov.

55. Schriver L, Schriver A, Perchard JP. Infrared Matrix-Isolation Study of the Molecular-Complexes Between Acetonitrile and Hydrogen Halides - Evidence for Reactivity Differences within the Halide Sereis. Journal of the Chemical Society-Faraday Transactions Ii. 1985;81(SEP):1407-25.

56. Computational Chemistry Comparison and Benchmark Database: https://cccbdb.nist.gov/

57. Buchberger AR, Danforth SJ, Bloomgren KM, Rohde JA, Smith EL, Gardener CCA, et al. Condensed-Phase Effects on the Structural Properties of FCH_2CN-BF_3 and $ClCH_2CN-BF_3$: A Matrix-Isolation and Computational Study. Journal of Physical Chemistry B. 2013;117(39):11687-96.

58. Popelier P. Atoms in Molecules: An Introduction. Harlow, England: Prentice Hall; 2000.

59. Parthasarathi R, Subramaniam V. Characterization of Hydrogen Bonding: From van der Waals Interactions to Covalency. In: Grabowski S, editor. Hydrogen Bonding - New Insights. Netherlands: Springer; 2013.

60. Phillips JA, Cramer CJ. B-N distance potential of CH3CN-BF3 revisited: Resolving the experiment-theory structure discrepancy and modeling the effects of low-dielectric environments. Journal of Physical Chemistry B. 2007;111(6):1408-15.

4

61. Bevitt J, Chapman K, Crittenden D, Jordan MJT, Del Bene JE. An ab initio study of anharmonicity and field effects in hydrogen-bonded complexes of the deuterated analogues of HCl and HBr with NH_3 and $N(CH_3)_3$. Journal of Physical Chemistry A. 2001;105(13):3371-8.